CURRENT SENSING SOLUTIONS FOR MODERN POWER ELECTRONICS

by

Hossein Niakan

A thesis submitted to the faculty of
The University of North Carolina at Charlotte
in partial fulfillment of the requirements
for the degree of Master of Science in
Electrical Engineering

Charlotte

2023

Approved by:

____
Dr. Babak Parkhideh

____
Dr. Robert Cox

____
Dr. Michael Mazzola

ABSTRACT

HOSSEIN NIAKAN. Current sensing solutions for modern power electronics. (Under the direction of DR. BABAK PARKHIDEH)

Power electronics facilitated the growth of a wide range of industries in today's world. Its presence can be seen in renewable energy systems, transportation electrification, smart grids, industrial drives, and consumer electronics to name a few. At the heart of the power electronics industry is the semiconductor, as power electronics rely on the semiconductor industry. With the advancements of wide bandgap semiconductor devices, many new power electronics solutions are becoming viable to realize and implement. Maintaining, prognostic, and protecting the aforementioned semiconductor devices require various compatible sensing solutions to enable intelligence and reliability. In this context, a novel sensing solution is proposed, designed, and implemented for modern power management systems. This sensing solution generates the current difference data of adjacent paralleled wide bandgap devices used within power modules of converters/inverters. This new dataset can be exploited with different topologies and machine-learning algorithms for prognostics and protection purposes. The concept is proven in this work through electromagnetic field simulation and analysis, as well as several experimental-level prototypes.

Besides maintenance, control and over-current detection are essential parts of all power electronic systems. Many high-efficiency and fast-response control and detection technologies are reliant on semiconductor switch current measurement. The accuracy and speed of such employed current sensors would dictate the performance of the overall system, consequently, for modern power electronics, compatible switch current sensing solutions need to be researched and developed. On this matter, a novel unidirectional Rogowski switch current sensor is proposed, developed, and tested in the scope of this work. The prototyped switch current sensor is capable of measuring

the fast switching current of wide bandgap semiconductor devices, including a novel compensation technique for DC measurement errors.

Both proposed sensing solutions are well promising to help create reliable and intelligent power management systems.

DEDICATION

I would like to dedicate this master's thesis to the steady support and encouragement of my family. Their love, understanding, and belief in my abilities have been the driving force behind my pursuit of higher education. This dedication is also extended to my exceptional advisor, Dr. Babak Parkhideh, whose expertise and guidance have shaped my academic and intellectual growth. Lastly, I dedicate this thesis to all the individuals who share a passion for the subject matter. May this work contribute to the existing knowledge and inspire future researchers in their quest for understanding and innovation.

ACKNOWLEDGEMENTS

I would like to express my deepest gratitude to all those who have supported and contributed to the completion of this thesis. I am immensely thankful to my advisor Dr. Babak Parkhideh, as well as my esteemed committee memebrs, for their support throughout the entire research process. Their valuable insights and constructive feedback have been instrumental in shaping this work. I would like to also acknowledge the financial support and facilities provided by the UNC Charlotte Department of Electrical and Computer Engineering and Energy Production and Infrastructure Center (EPIC). This material was supported by the National Science Foundation under Award No. 1610250, as well as Army Research Laboratory (ARL).

TABLE OF CONTENTS

LIST OF TABLES

LIST OF FIGURES

LIST OF ABBREVIATIONS

AC	An acronym for Alternating Current.
AI	An acronym for Artificial Intelligence.
AMR	An acronym for Anisotropic Magneto-Resistive.
CMC	An acronym for Current Mode Control.
CMOS	An acronym for Complementary Metal-Oxide Semiconductor.
CMRR	An acronym for Common Mode Rejection Ratio.
CT	An acronym for Current Transformer.
DC	An acronym for Direct Current.
EMI	An acronym for Electromagnetic Interference.
FET	An acronym for Field Effect Transistor.
GaN	An acronym for Gallium Nitride.
GMR	An acronym for Giant Magneto-Resistive.
HEMT	An acronym for High-electron-mobility Transistor.
IGBT	An acronym for insulated-Gate Bipolar Transistor.
MOSFET	An acronym for Metal Oxide Semiconductor Field Effect Transistor.
MR	An acronym for Magneto-Resistor.
Op-Amp	An acronym for Operational Amplifier.
PCB	An acronym for Printed Circuit Board.
PMSM	An acronym for Permanent Magnet Synchronous Motor.

RCCS	An acronym for Rogowski Coil Current Sensor.
RSCS	An acronym for Rogowski Switch Current Sensor.
SiC	An acronym for Silicon Carbide.
SMD	An acronym for Surface Mount Device.
SRM	An acronym for Switch Reluctance Motor.
TMR	An acronym for Tunnel Magneto-Resistive.
WBG	An acronym for Wide Bandgap.

PREFACE

Current sensing is an essential aspect of power electronics, as it allows for monitoring and controlling the flow of electrical current in various systems [5, 6]. Such sensors play a critical role in applications such as dc-dc power conversion and adjustable speed motor drives [7, 8]. The dynamic performance and control of these systems rely on the accuracy and efficiency of their sensors. Achieving accuracy in current sensing is essential to optimize the performance and energy efficiency of power electronics [9, 10]. A variety of current sensing methods are available, including conventional approaches like the shunt resistor, current transformers (CT), and Rogowski coils; as well as magnetic field detectors such as magneto-resistors, hall-effect, flux-gate, and hybrid technologies. Some of these technologies are evaluated and compared based on their capacity for lossless sensing, simplicity, and ease of implementation [5, 6, 11].

Switch current sensing is a commonly used technique in power electronics, especially in switch-mode power supplies. This technique involves measuring the current flowing through a switch to control, protect, and characterize the device under monitoring [12, 13, 14]. Switch current sensing has several advantages over other current sensing techniques such as providing fast response times and high accuracy, making it well-suited for high-frequency and precise protection and control applications.

One of the most popular methods for switch current sensing is based on the use of shunt resistors. Shunt resistors are low-resistance elements placed in series with the switch, and the voltage across the resistor is measured to determine the current flowing through the switch. The voltage drop across the shunt resistor is typically very small, on the order of a few millivolts, and requires a high-precision amplifier with a high common-mode rejection ratio (CMRR) to obtain accurate measurements. Shunt resistors are almost often only used to measure a low-side source/emitter current of a switching device, as they are not galvanically isolated. Moreover, these sensors/probes add excessive parasitic and deteriorate the device/system efficiency and performance.

Another method for switch current sensing is based on the use of magnetic sensing elements, such as Hall-effect and magneto-resistive (MR) detectors. Hall sensors use the principle of the Hall effect to measure the magnetic field produced by the current flowing through the switch. Similarly, MR sensors consist of Wheatstone bridges working based on principles of magneto-resistance effect. These sensors' output voltage is proportional to the current flowing through the switch, and the voltage can be amplified and processed to obtain an accurate measurement of the current. The bandwidth of such sensors would cover DC and be limited to around 5MHz [5]. Additionally, magnetic element sensors can be affected by external magnetic fields (EMI), which can lead to inaccuracies in measurements.

Rogowski coil current sensing is another widely used technique in power electronics. This approach involves measuring the current flowing through a conductor by measuring the voltage induced in a coil placed around the conductor. The voltage induced in the coil is proportional to the rate of change of the current flowing through the conductor (Faraday's Law) and can be integrated to obtain an accurate measure of the current. One of the main advantages of Rogowski coil current sensing is that it does not require physical contact with the conductor being measured. This makes it well-suited for high-voltage and high-current applications where safety is a concern. Additionally, Rogowski coil current sensing has a wide frequency range, making it suitable for high-frequency applications. Nevertheless, Rogowski coil current sensing has some disadvantages as well. These sensors have no response to non-varying (DC) components of magnetic fields. As such, they are mainly used in purely AC waveform measurement. Specifically, in switch current measurement applications, several advanced approaches are taken to overcome the lack of DC measurement issues [13, 14, 15, 16, 17]. Yet, these approaches are either too complex or not suitable for megahertz switching frequency applications.

In this work, two different current sensing technique is proposed, studied, and evaluated. The initial concept involves a single-axis magnetic field detector integrated with high-frequency switching devices to measure the current difference between each pair of adjacent paralleled switches. This novel data collection method opens the door for several research opportunities to develop protection and prognostic algorithms around. The second approach involves a PCB-embedded Rogowski coil sensor consisting of a novel DC compensation auxiliary circuit for uni-directional switch current measurement applications. The proposed sensor shows extremely high performance in measuring the high-side switch current of a SiC half-bridge module. In upcoming chapters, details of each proposed sensing technology would be discussed further.

CHAPTER 1: LITERATURE REVIEW

Current sensing is a crucial aspect in power electronics, from protection to, prediction and prognostics, to device characterization, and motor control. In protection applications, current sensors are used in order to measure the current flowing through power devices, detecting overcurrent, short-circuit, or ground faults which are vital to ensuring safe, efficient, and reliable operation and control. Across prediction and prognostics, current sensors are not only used to monitor the health of power electronic components but also to predict their remaining useful life. In device characterization, current sensors are used to measure the electrical properties of electronic devices, whilst, in motor control, high-accuracy current sensing is imperative for achieving smooth and efficient motor operation, reducing energy consumption, and extending the life of the motor.

As a result of the research community's focus to provide accurate, fast, reliable, and integrable current sensing solutions that serve the newly developed, and legacy power electronic systems alike, various types of current sensors have been designed and integrated with power electronics for different applications, including sensors such as the magneto-resistors (MR), current transformers (CT), Rogowski coil, and contactless Hall Effect.

Several types of current sensors have been designed and integrated with power devices for different applications, including those in protection applications. In such applications, sensors are used to measure the current through the power devices whilst detecting overcurrent, short-circuit, or ground faults. Fault detection is paramount in ensuring safe and reliable power electronics operation, preventing damage to the devices, and at the same time, protecting the user from any potential hazards.

An example of this is a giant-magneto-resistive (GMR) sensor that has been integrated with the gate driver of a planar IGBT power module which provided information related to over-current protection [18]. Following this, [19] shows a tunnel-magneto-resistive (TMR) being used in a 1200V/200A IGBT module for over-current detection, as well as DC bus capacitance estimation. This specific integrated sensor sub-circuit has 1.23us protection, as well as 677ns short-circuit fault detection response. Whilst the author of [20] has also used a tunnel-magneto-resistive (TMR) sensor, in this case, the sensor was used to provide over-current and short-circuit protection for a silicon carbide (SiC) power module. In other examples such as [21], the author designed a 1200V/300A SiC power module with embedded Rogowski coil current sensors for short-circuit detection alongside phase current measurement.

As well as this, authors for both [22] and [23] integrate a Rogowski coil sensor into a single-switch DC-DC converter to measure the inductor current derivate. This information is used for fault detection and capacitor life monitoring. An ultra-high-frequency AC current sensor is used in [24], to measure the decoupling capacitor current of a high-frequency converter. This information is used for short-circuit protection. Another Rogowski coil sensor is used in [25]. However, in this case, it is integrated with a SiC MOSFET device to measure the switch current. This information is then used for over-current detection through a novel gate-source shorting toggle mechanism.

Moving from the use of current sensing in protection applications to its role in prediction and prognostics. Prognostic and predictive maintenance strategies are becoming increasingly popular in power electronics as they enhance system reliability and reduce downtime. Current sensors are widely used in these strategies to monitor the health of power electronic components while predicting their remaining useful life. One such example is detailed in [26] the author developed an ageing detection scheme for SiC MOSFET devices, by measuring the gate leakage current. This leakage current sensor is mainly a low-power electronic sub-circuit, which provides enough information to allow it to be used as an ageing precursor.

[27] details another application of current sensing in power electronics is in high-voltage power module protection and current monitoring with the development of a PCB-embedded Rogowski coil. This solution is compact, accurate, and inexpensive for such applications. The author of [28] takes a similar approach and uses a PCB-embedded Rogowski coil sensor, but in this case, it is to measure the individual chip currents of a press-pack IGBT module. This information is used to provide feedback for the balancing of the paralleled chips on the IGBT power board.

In [29], the author designed a compact Rogowski coil sensor to be integrated with high-frequency SiC modules. The sensor is used to provide information for active current balancing of the paralleled devices. The proposed sensor has a bandwidth of 2.66Hz – 100MHz.

As we move away from the use of current sensing in prediction and prognostics, to its use in device characterization, we can see current sensors play a significant role in measuring the electrical property of electronic devices. The exact choice of the current sensor depends on the specific application and properties being measured. For example, the author of [30] proposes using a silicon steel current transformer for the characterization of fast-switching power semiconductors. The sensor is tested and validated on both a discrete SiC, as well as a 1000A discrete IGBT device.

[31] details the design of a co-axial current transformer (CCT) being used to minimize current monitoring insertion impedance. This sensor is used to characterize the fast switching IGBTs with less than 30ns switching times.

In [32], the author has proposed two hybrid DC – 50MHz sensor current probes to be used for high-frequency power electronics measurements. The probe consists of both a current transformer (CT), in addition to a Hall Effect sensor. The design includes a shielding method for the Hall sensor to avoid electromagnetic interference.

In addition, [33] shows a designed 1.6 GHz SMD shunt current probe. The application of this specific sensor is for high-frequency wide bandgap semiconductors characterization. This sensor is shown to have insertion inductance as low as 10 pH.

As well as its use in device characterization, current sensing plays a pivotal role in motor control applications, such as variable speed drives, robotics, and electric vehicles. In such systems, current sensors are used to measure the current flowing through the motor windings and provide feedback to control the motor speed and torque. High-accuracy current sensing is vital for achieving; efficient and smooth motor operation, reducing energy consumption, and extending the life of the motor.

A 50A contactless Hall Effect sensor with a DC-200KHz frequency detection range. (LA-55P) is used in [34]. This sensor measures the sum of all three phase currents (DC-link current) to provide feedback control for a switched reluctance motor drive. The authors of [35] also used a 50A non-invasive Hall Effect current sensor with an accuracy of %1, and an upper limit bandwidth of 50KHz. This current sensor is utilized to measure the phase current of a 3-phase inverter, controlling a permanent magnet synchronous motor (PMSM).

Meanwhile, in [36], a Hall Effect current sensor is used to measure the DC-link current for control of a dual switch reluctance motor (SRM) drive system. The measured current is then used to reconstruct all three phases of currents for each SRM.

A novel approach is taken in [37] to; develop a more credible control mode or a fault-tolerant control strategy for permanent magnet synchronous motors (PMSMs), without requiring any position sensors, while using a single current sensor for the feedback system. The sensor used in this work to measure the phase current is a 15A flux gate detector with 300 KHz 3-dB bandwidth and an accuracy of %0.8.

Current sensing is not only vital in motor control but also very fundamental for power supply applications, such as AC-DC converters and DC-DC converters. In these converters, the current flowing through the power devices is measured and used to regulate the output voltage and current. Accurate current sensing is essential to ensuring stable and reliable power supply operation, reducing power losses, and improving efficiency. One control scheme that uses switch current measurement information in power electronics is current mode control (CMC).

An on-chip CMOS current sensor is integrated with a DC-DC buck converter for instance in [38] to provide the information for current mode control. The DC-DC converter and current sensor are both manufactured in a 0.35um CMOS process. Similarly, in [39], the same on-chip CMOS current sensing is integrated with the addition of dynamically-biased shunt feedback. This allows for current mode control for high-frequency DC-DC converters.

Other studies such as [40] detail the author manufacturing a DC-DC converter with an integrated CMOS current sensor on a 0.5um process, which is to be used for current mode control algorithms. While in [41], the author designed a novel current sensor in 0.18um CMOS process, which is suitable for high-voltage DC-DC converter control. This design includes a switch capacitor differentiator and voltage-to-time converter, as parts of the on-chip current sensor. Additionally, a sense-FET is integrated with a DC-DC buck converter in a 0.18 um CMOS process in [42]. This sensor is designed to detect the inductor current with a relatively wide dynamic range.

While current mode control (CMC) is widely used for current sensing in power electronics, another type of current mode control known as Peak current mode control (PCMC) is also used in switching power supplies to sense and control peak inductor current. PCMC with slope compensation provides a variety of advantages such as automatic input line feed-forward, inherent cycle-by-cycle overload protection, and current sharing capability in multi-phase converters.

A sense-FET high-side current sensor is designed in a 130 nm CMOS process in [43]. This sensor is integrated with a 40V 3MHz DC-DC converter for peak-current control. As a result of the fast response of the sensor, the converter minimum on-time is reduced to 51ns. Also, a MOSFET sensing block is integrated with an asynchronous DC-DC boost converter throughout [44]. This specific sensor monitors the output current of the converter with a wide current range.

This is while[45] shows the design of an indirect inductor current sensor and its implementation for a floating ground buck-boost converter. This sensor provides real-time peak-current detection for a 2MHz flying-capacitor GaN DC-DC converter.

In [46], a high bandwidth cascade current transformer (CT) is designed for measuring fast current transients of power electronic components. The sensor proposed in this work can achieve an upper bandwidth of 70MHz. The author of [47], has also designed a current transformer (CT) for in-situ current measurement of discrete SiC switching devices. This design combines a current probe and the CT for bandwidth extension. Moreover, they have studied the impact of core material on the characteristics of the sensor.

Since current mode control offers an improved transient response and stability compared to voltage mode control, it is commonly used in high-performance power converter applications. This implies, the higher the switching frequency, the higher bandwidth and slew rates are required on the sensor technology. Contactless current sensors have gained significant attention in recent years due to their non-invasive nature, high accuracy, and safety advantages compared to traditional current sensors. On this matter, the author in both [11][15] and [12][16], designed a contactless sensor that could be suitable for high-frequency power converter designs. The hybrid DC-10MHz current sensor is comprised of a PCB-embedded Rogowski coil and an anisotropic magneto-resistive (AMR) element.

The authors in [48] propose a hybrid sensor design for integration with wide bandgap power converters. This sensor has an extended upper bandwidth of 20MHz and is designed to have very high electromagnetic interference immunity. The sensor is also tested in WBG power converter utilizing GaN Systems switching devices.

A PCB-embedded differential Rogowski coil sensor was the approach taken in [49]. The sensor is; used to measure the device current of next-generation power electronics and utilizes differential properties to mitigate the capacitive coupling of the coil. In order to improve the performance of the sensors for contactless low-current high-frequency signals, the author of [50] proposes a new coil and a Hall Effect plate design.

On the other hand, the authors of [51] and [52], have designed a hybrid DC-50MHz current sensor comprising PCB-embedded pickup coils and a Hall Effect element. This sensor is used to measure the inductor current for closed-loop control of a 4.8MHz three-level triple-interleaved flying capacitor GaN converter. Similarly, The author of [13] opts to design a DC-75MHz hybrid sensor using an on-chip Rogowski current detector on a 180nm CMOS process. By doing so, this work extends the lower band detection range by integrating an additional Hall Effect sensor.

A methodology to integrate a PCB-embedded Rogowski coil sensor with a 48V GaN DC-DC converter is proposed in [53]. The designed Rogowski coil has an upper bandwidth of larger than 500MHz, measuring the transistor and phase currents. As well as this, shielding possibilities to improve the sensor performance were also studied in this work.

On applying such current sensors, the author in [54] uses a current sensor in order to implement a current sharing control method for bidirectional interleaved DC-DC converters. The sensor and methodology evaluation is performed on a 300W three-phase bidirectional interleaved DC-DC converter test bed.

On the subject of current sensors in advanced converters, there's a noticeable trend in recent designs, as current sensors are often integrated with the module gate driver sub-system. Within this context, the authors of [14], designed a Rogowski switch current sensor (RSCS) that is integrated with the gate driver circuitry. This sensor provides switch current information of the devices on a 10kW, 240A SiC power module. Moreover, the authors provide enhanced temperature compensation for this sensor [17].

A sense-HEMT structure is monolithically integrated as part of a 650V totem pole PFC GaN gate driver and this sensor achieved a 2500:1 sensing ratio while imposing minimum loss [55]. As per both [56] and [57], a Rogowski coil current sensor (RCCS) is integrated with the gate driver of a 211 kW SiC three-level aircraft propulsion inverter. The integrated current sensor is used for suppressing overshoot voltage, ultra-fast short-circuit protection, and ac load current sampling [58].

While in [59] and [60], the author provides a Rogowski coil sensor design for short-circuit protection of a 1.7 kV SiC power module. This sensor is integrated with the gate driver circuit board of the power module including an auxiliary processing circuit.

It's important to note semiconductors are crucial components of modern electronic devices, and as such, an accurate measurement of their properties is paramount for the development and improvement of these devices. Switch current sensing is a vital aspect of many power electronic applications including overcurrent protection, renewable energy systems, current mode control, motor control, and fault detection. The choice of the current sensor depends on the specific application, including aspects such as environmental conditions, the current range, and accuracy. The continued development of switch current sensing technology will be crucial for the advancement of energy-efficient and sustainable power electronics.

On this matter, a PCB-embedded Rogowski coil is designed and used for a GaN half-bridge module in [61]. The sensor measures the switch current information with high accuracy, which would be required for transient current measurements.

While in [62], the author designed and implemented a Rogowski coil sensor to measure the switch current of SiC MOSFETs in a 1.7 kV power module. This sensor not only provides the necessary data for short-circuit protection but also the current control of the module. The Rogowski switch current sensor utilizes periodic auxiliary discharge circuitry for the integrator capacitor to compensate for the lack of DC measurement.

The author of [63] proposed a differential compensation scheme for Rogowski switch current sensors which are used inside the power modules. In doing so, this solution helps to lower the cost and burden of using an auxiliary circuit similar to [62] for DC compensation.

In [64], the author has designed an integrated switch current sensor for GaN power devices. This is a single-turn coil detector and is used to measure the device current for estimation of its characteristics. Sensor performance is experimentally verified on a 40V/25A GaN double pulse test setup.

CHAPTER 2: CURRENT DIFFERENCE MEASUREMENT

2.1 Background

The ability of a system to perform its required tasks within a specified timeframe is known as reliability [65]. Although Wide Band Gap (WBG) devices have superior characteristics that allow for higher power density compared to Silicon and IGBT designs, the overall reliability of such high-frequency systems is crucial for achieving optimum performance. A variety of diagnostic, protection, and control methods have been studied in [10, 19, 20, 21, 22, 23, 24, 25, 26, 27, 59, 60, 62, 66, 67, 68, 69], to ensure reliability. Additionally, authors in [70] suggest using Kalvin connection, advanced layout packaging, and die arrangements for optimized multichip power module performance. Other proposed methods detailed in [71, 72] involve monitoring power devices based on their case temperature. Auxiliary monitoring/protection units, such as planar Rogowski coils integrated with the gate-driver of SiC modules for short circuit detection and phase current reconstruction were studied in [59, 60, 62, 73], as well as voltage measured over the parasitic inductance as shown in [68]. Furthermore, an IoT scheme such as the one proposed in [69] allows for remote and automatic actuation in power converters based on the degradation levels of their power devices.

Balanced current sharing between paralleled devices is a crucial aspect of power module reliability as emphasized in [28, 29, 74, 75]. The power switch is the primary component of each power module, requiring optimum performance conditions to be enforced on each device to greatly improve the overall performance and reliability of the system. Unequal distribution of system layout/parasitics can result in imbalanced current distribution, which in turn can be caused by an imbalanced R_{DS-ON} distribution between paralleled devices due to ageing or manufacturing processes. The dynamic current imbalance between paralleled dies can limit the overall maximum current rating and thermal stability of the power modules [29, 71, 74, 76]. Multi-paralleled WBG modules require well-designed protection, control, and prognostics sub-systems for optimal reliable performance, which require various condition monitoring nodes.

The symmetrical layout design of power modules allows for a predictable magnetic flux around lateral GaN HEMT devices due to their two-dimensional electron gas (2DEG) charachteristics, which differs from vertical current conducting devices [1]. This inherent feature, along with lateral device packaging, enables the integration of single-axis point field detectors in proximity of the switching device. This chapter proposes an innovative condition monitoring element integrated with a high-frequency GaN power module to obtain data about the module's current distribution. To successfully implement this integration, an understanding of the magnetic field behavior in the module chamber and several additional layout optimizations are required [74, 76].

2.2 Current Difference Measurement Concept

The widespread adoption of wide-bandgap semiconductor devices has revolutionized the power electronics industry, resulting in a higher frequency of operation, smaller footprints, as well as more compact packaging. The latest state-of-the-art high power-density modules deliver higher efficiency, but it is imperative they are maintained at their optimum operating condition. Monitoring various module operating parameters such as V_{DS}, R_{DS-ON}, I_D, and module temperature can also help to ensure proper semiconductor operation in modern power modules. In order to achieve higher power density, designers tend to parallel and series the wide-bandgap devices in various applications. Nevertheless, it is crucial to ensure the equal sharing of current between all of the paralleled semiconductors to achieve optimum operating conditions. Therefore, device current measurement is one of the most crucial factors to ensure module reliability and efficiency [1].

As explained in [2], a novel way to measure individual device current is to measure the current mismatch between each pair of paralleled semiconductors. This concept is verified using finite element simulations, also to locate the appropriate placement for a point field detector to sense the current mismatch between a paralleled GaN configuration. Subsequently, the concept is experimentally validated, using a various detectosr for planar GaN modules.

Based on the results shown in [2], during the conduction cycle, the MR sensor detects a calibrated zero (~2.5V), while both of the paralleled GaN devices share the current equally. This occurs because the MR location and module layout are designed so that the impact of the magnetic field created by each lateral conducting semiconductor is equal and opposite on the sensor, given the equal current sharing condition [1]. Although the AMR detector has a relatively small footprint and provides essential data, its current handling capability is essentially twice as effective, since measuring the current difference (and not the absolute current). Furthermore, the frequency of operation limits most of the advanced families of MR technology today, hence a coil detecter is also experimented and analyzed. Nonetheless,as also reported in [2, 3, 1], the current mismatch measurement concept is experimentally proven for up to 20 Amperes of module current difference.

2.3 Electromagnetic Field Simulations

Given a balanced operating condition, the imbalanced current distribution of the system could be majorly caused by unequal distribution of system parasitic and layout. Typically, this parasitic imbalance would be a direct result of a Printed Circuit Board (PCB) design. While unbalanced current distribution can also be caused by imbalanced R_{ds-ON} distribution between paralleled devices. Therefore, it is crucial to provide a symmetric board layout with respect to switching devices (hypothetically, the same device characteristics are considered for devices from the same batch), in or-

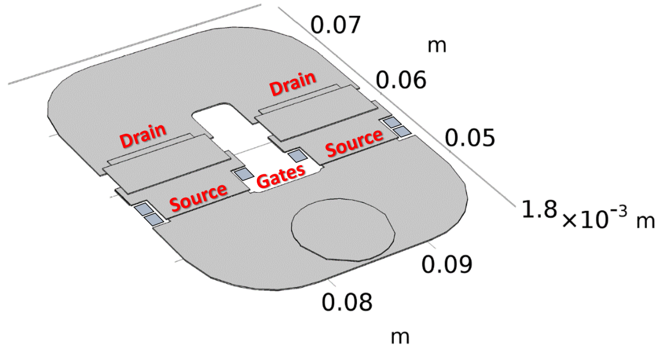

Figure 2.1: 3D geometry of the 2-die GaN power module conducting layer.

der to equalize the current sharing of the paralleled devices. Provided the symmetric circuit layout design, the two-dimensional current conduction of GaN devices allows a much more predictable magnetic flux created around traces and device, as opposed to vertical current conducting devices. Consequently, these devices are suitable to be integrated with point field detectors as proposed in this chapter.

The two-dimensional electron gas (2DEG) structure of such GaN MOSFETs enforces these devices to conduct current in a lateral manner. The geometry, which is shown in Figure 2.1, was developed for the simulation of two parallel GaN devices in a CAD desiging tool. In this geometry, the dimensions were adapted to the ones from actual dimensions.

The purpose of this simulation set is to use COMSOL Multiphysics simulation tools to study the magnetic field distribution around a current carrying module consisting of two GaN HEMTs dies in parallel (shown in Figure 2.1). In order to construct the main physical geometry base, the module layout was designed in Allegro PCB designer utilizing the packaged GS66516B GaN footprint from GaN Systems. GS66516B packaging allows easier prototyping process, as well as similar pin-layout configuration compared to its die version (GS-065-080-1-D). Die footprint is 40% smaller than the packaged product. Then, the single-layer layout was exported appropriately into COMSOL Multiphysics.

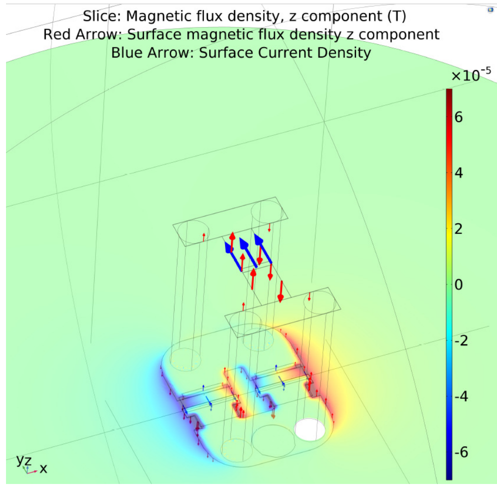

Figure 2.2: Color plot of magnetic flux density (z-component) on a specified 3D slice [1], © 2020 IEEE.

After importing the main geometry, module ports were located and extruded, as well as the current excitation port. An AC current excitation port with zero phase shift (initially) and zero offset is implemented as the main power source of the loop. The current flows into the drain, passes through the drain-source channel (with defined R_{DS-ON}), and lastly flows back into the negative terminal from the source of both devices.

After finalizing the simulation setup, the magnetic field distribution around this module has been studied for various frequencies, currents, and R_{DS-ON} conditions. Figure 2.2 displays the color plot of the magnetic flux density (z-component) due to an AC current of 1 Ampere amplitude oscillating at a 100 KHz frequency rate. R_{DS-ON} values for both GaNs are set to 25 mΩ in this set of simulations.

In order to examine the magnetic flux density in detail, various 3D cut lines have been defined over the area of interest (sensor location), which is about 3.56mm by 6mm in area. These cut lines can be seen in Figure 2.3, indicated in red. The 3.56mm by 6mm region is covered with 60 equally distanced 3D cut lines. For the purpose of sensitivity evaluatoin, a single-turn z-axis coil is assumed to be covering the targeted area. The z-component of the magnetic field in this region would induce a voltage

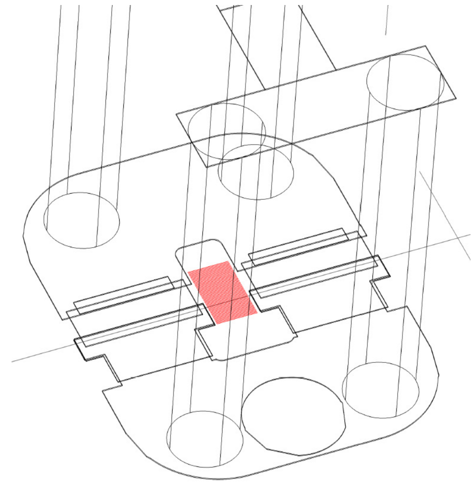

Figure 2.3: Multiple 3D cut lines defined in space, covering the location designated for a z-axis magnetic sensor [1], © 2020 IEEE.

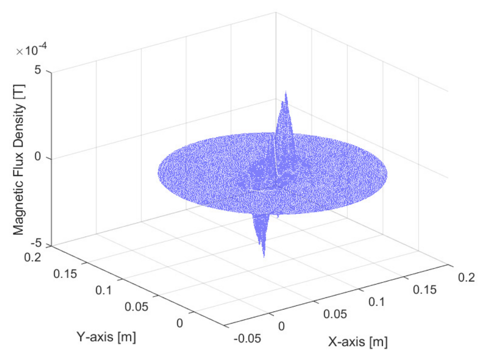

Figure 2.4: Magnetic flux density (B) distribution over the specified cut plane

across the ends of a single-turn coil covering that area.

The simulated magnetic flux density (B) data were next exported for further analysis. Figure 2.4 shows the z-component of magnetic flux density distribution over the predefined 3D cut plane.

In the following figure, magnetic flux density distribution along the defined 3D cut lines shown in figure 2.3 are plotted. Figure 2.5 shows the magnetic flux density over the defined (red) area. As the ON-resistance of both devices have been set to 25 mΩ, it can be observed that this distribution is symmetrical around xy-plane. Hence, the surface integral of the magnetic field over this region (having balanced current

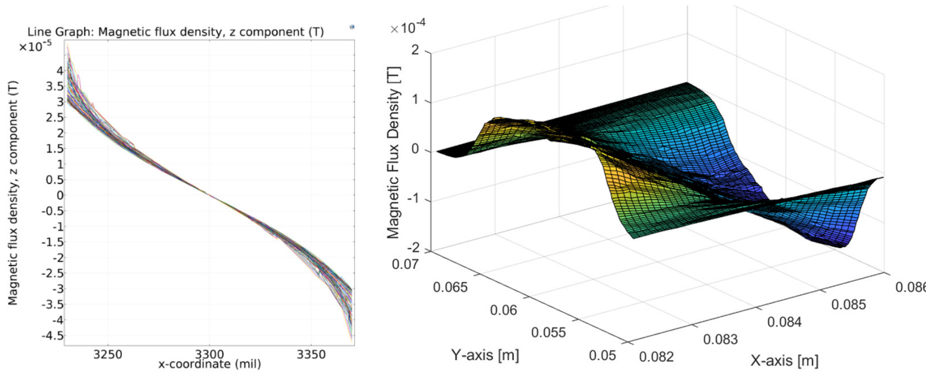

Figure 2.5: Magnetic flux density due to balanced current conduction. Left: Magnetic flux density (B) for various specified 3D cut lines. Right: Magnetic flux density (B) distribution plotted in 3D [1], © 2020 IEEE.

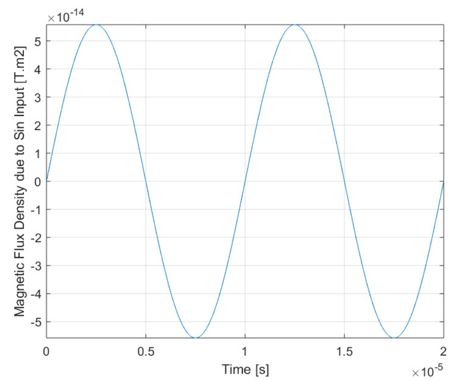

Figure 2.6: Time varying magnetic flux (φ) due to sine wave excitation

distribution) is theoritically zero.

On the other hand, the magnetic flux (φ) for the specified area, is calculated by simulation and its waveform is depicted in figure 2.6. In this calculation, first, the line integral of all of the graphs in Figure 2.5 is calculated and added together. Then, considering the y-axis step size, the final value of flux density is calculated.

Now, in order to extract the voltage induced on a single-turn coil, the following relation would be considered:

$$V_{INDUCED} = -\frac{d_\phi}{d_t} \tag{2.1}$$

Hence, figure 2.7 shows the induced voltage due to sine input.

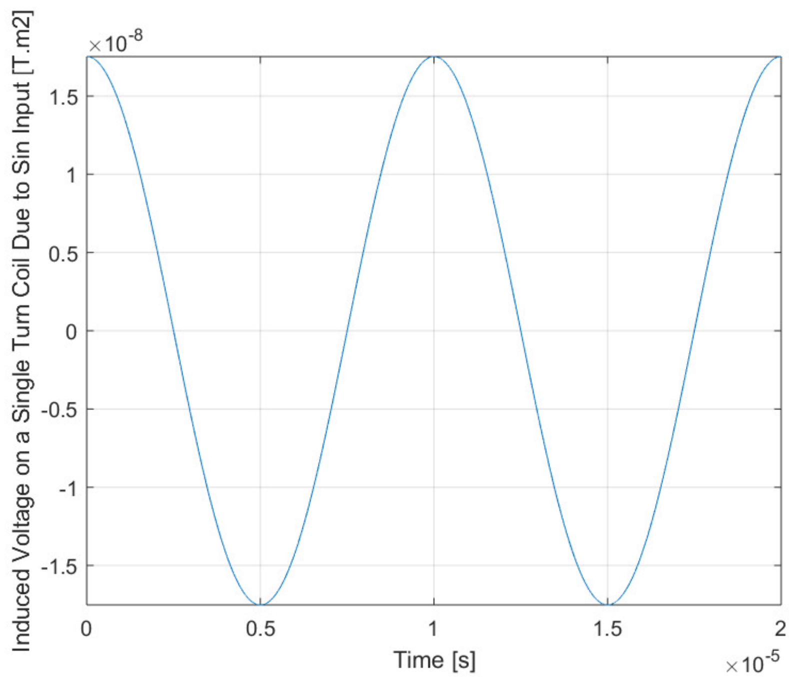

Figure 2.7: Induced voltage due to sine current input

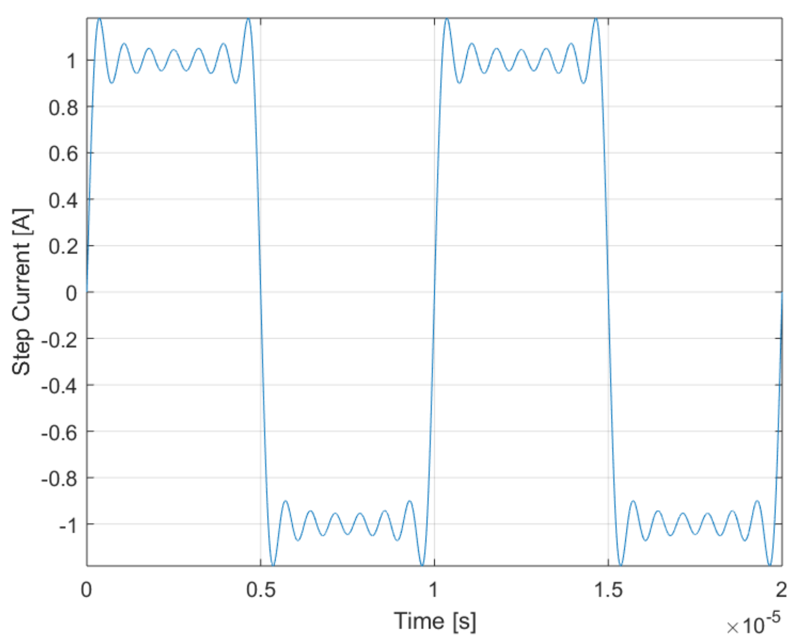

Figure 2.8: Pulse current input

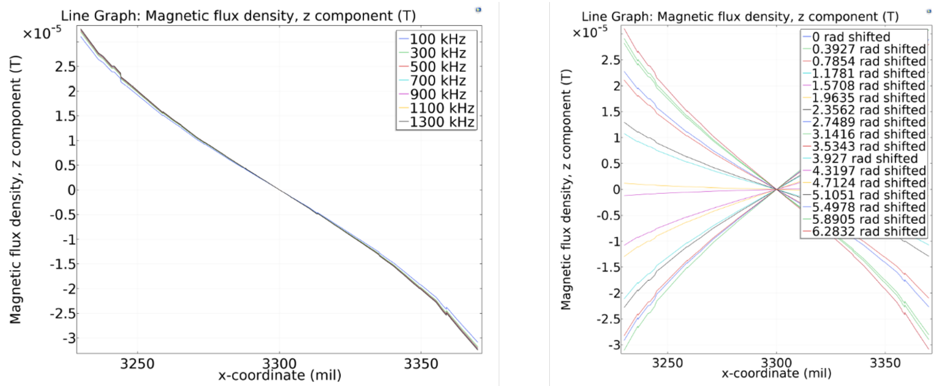

Figure 2.9: Magnetic flux density (B) distribution for a single 3D cut line swept over various frequencies and phase shifts of the input sine wave.

Now that the voltage induced for sine wave input is simulated and calculated, using superposition, as well as Fourier series expansion, the square-wave shown in Figure 2.8 was constructed as the input current. Each sine component of this input is seperetaly simulated and the data is gathered. Magnetic field distribution data of these sets of simulations were plotted in Figure 2.9. Each of these lines are essentially the z-component of the magnetic field for a single cut-line over different frequencies and phaseshifts due to a 1A sine wave input.

Based on the simulation for the first seven components of the square-wave Fourier series expansion, the final varying magnetic flux density due to the square wave shown in Figure 2.8 is calculated and graphed Figure 2.10. Moreover, the induced voltage due to the current waveform shown in Figure 2.8, is calculated and depicted in Figure 2.11. Based on this set of analysis, a single turn coil sees spikes of absolute value 67 nV, during transients for a fully balanced current distribution. This value is very small and close to zero as expected from the theory. Therefore, a fully balanced current distribution insertes virtually zero z-axis magnetic field over the area depicted in red in Figure 2.3.

In order to characterize the sensitivity of the coil located in the aforementioned area, it is required to simulate the magnetic field for an imbalance current distribution. The first scenario considered is when one of the dies (left die) is completely considered as

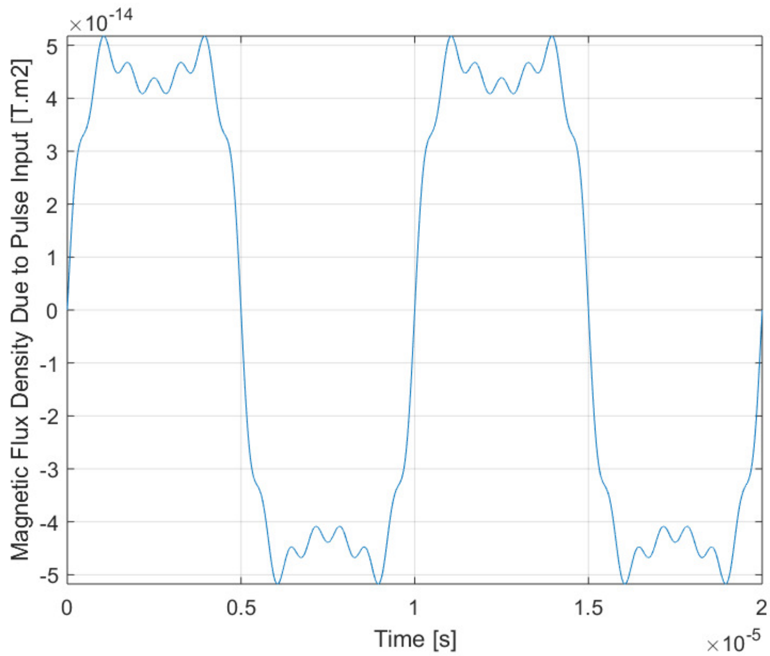

Figure 2.10: Varying magnetic flux due to the square-wave current shown in Figure 2.8.

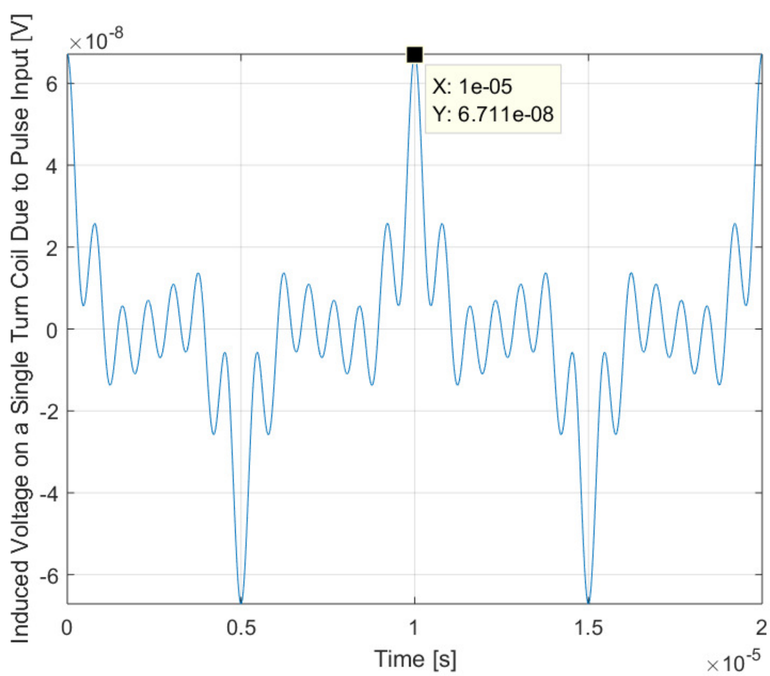

Figure 2.11: Induced voltage on a single-turn coil having the balanced current distribution.

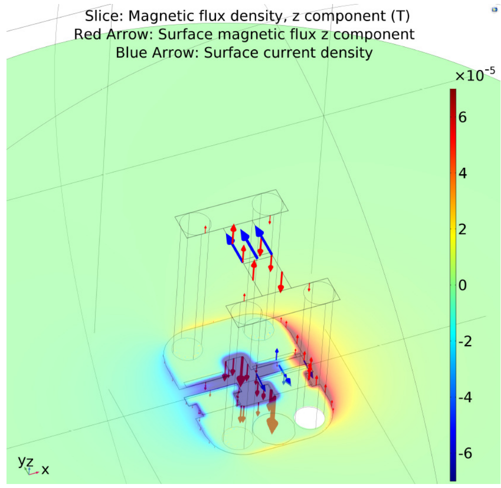

Figure 2.12: Color plot of magnetic flux density (z-component) on a specified 3D slice for imbalanced current distribuition of 1A [1], © 2020 IEEE.

an open circuit. Similar to the previous section, the z-component of the magnetic flux density is color-plotted for an AC current of 1 Ampere amplitude oscillating at 100 KHz frequency rate. R_{DS-ON} value for right GaN is set to 25 mΩ, and Left GaN is left open-circuit. Moreover, in order to examine the magnetic flux density in detail, various 3D cut lines have been defined over the area of interest as shown before in Figure 2.3. Figure 2.12 shows the magnetic field distribution for a specified cut-plane for this imbalance current distrubuted simulation.

In the following figures, this magnetic flux density (z-component) distribution along the defined 3D cut lines are plotted. Figure 2.13 shows the magnetic flux density over the defined (red) area in 2D and 3D. It can be observed that this distribution is not symmetrical along the xy-plane.

As explained in the previous section, time-varying magnetic flux as well as induced voltage are calculated following the same procedure. Similarly, using Fourier series expansion, the induced voltage due to a square wave input shown in Figure 2.14 was calculated and plotted base on several sweeps of simulation. As can be seen in Figure 2.14, the induced voltage due to the current pulse of 1A oscillating around zero with 100 KHz frequency, is 12.63 mV.

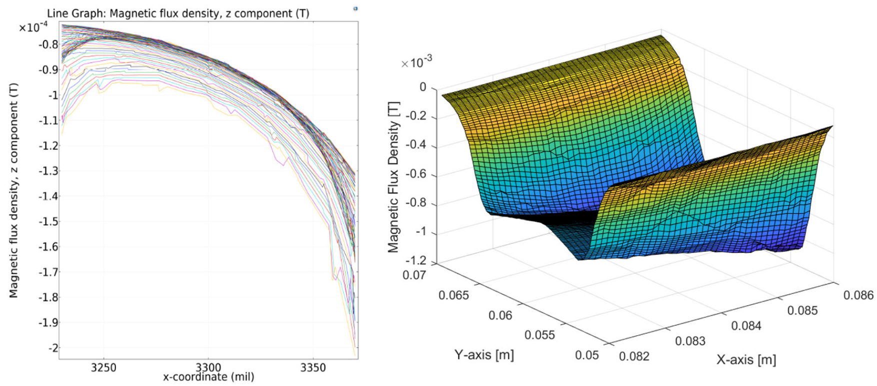

Figure 2.13: Magnetic flux density due to imbalance current conduction. Left: Magnetic flux density (B) for various specified 3D cut lines. Right: Magnetic flux density (B) distribution plotted in 3D [1], © 2020 IEEE.

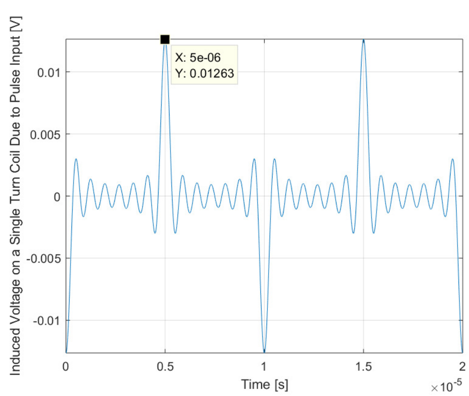

Figure 2.14: Induced voltage on a single-turn coil having the imbalanced current distribution of 1A. Left die set to open, and right die R_{DS-ON} at 25 mΩ

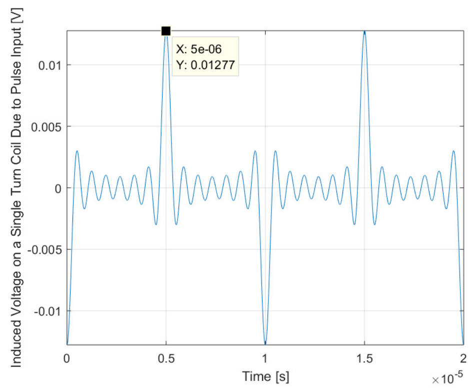

Figure 2.15: Induced voltage due to square wave input shown in Figure 2.8. Left die R_{DS-ON} set to 10 MΩ, and right die R_{DS-ON} at 25 mΩ (1A current difference)

In the next step, in order to confirm this value as a sensitivity of 1A current difference, simulation was done for two other scenarios that cause a 1A current mismatch between both conducting dies. Firstly, the left die, ON-resistance was set to 10 MΩ, while the right GaN was kept at 25 mΩ. The voltage induced due to 1A pulse current is depicted in Figure 2.15.

On the second scenario, the left die, on-resistance was set to 50 mΩ, while the right GaN was kept at 25 mΩ. The voltage induced due to the total module current of 3A is shown in Figure 2.16. From Figure 2.14-2.16, it can be seen that the induced voltage is around 12.63 mV, 12.77 mV, and 12.62 mV respectively. This conlcudes the validation of these sets of simulations to prove the current mismatch concept and define magnetic field behaviour over the targeted sensor placement area.

Lastly, the single-sided module with the right die set at 25 mΩ was simulated with 10A pulse input current, and its effective induced voltage is depicted in Figure 2.17. The induced voltage value for 10A current is 128.3 mV. This shows the linear relationship between the amplitude of the device current and the magnetic field strength created around the current carrying device.

The simulation studies in here demonstrate that a single turn coil with a dimension of 3.56mmx6mm, positioned in the specified area, has a sensitivity of approximately

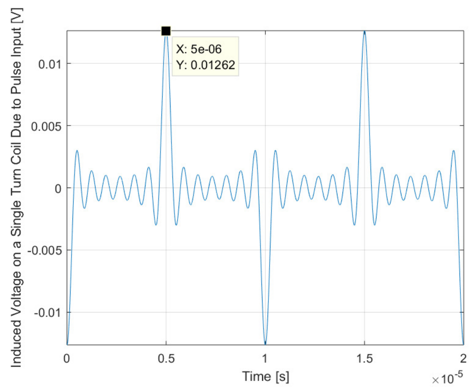

Figure 2.16: Induced voltage due to square wave. Left die R_{DS-ON} set at 50 mΩ, and right die R_{DS-ON} at 25 mΩ (1A current difference)

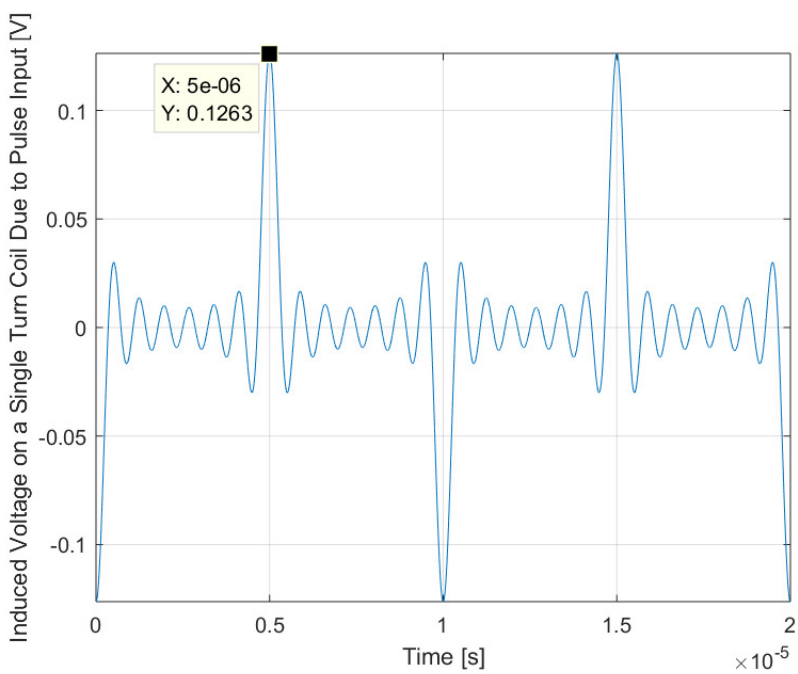

Figure 2.17: Induced voltage due to square wave, left die as open circuit, and right die at 25 mΩ (10A current)

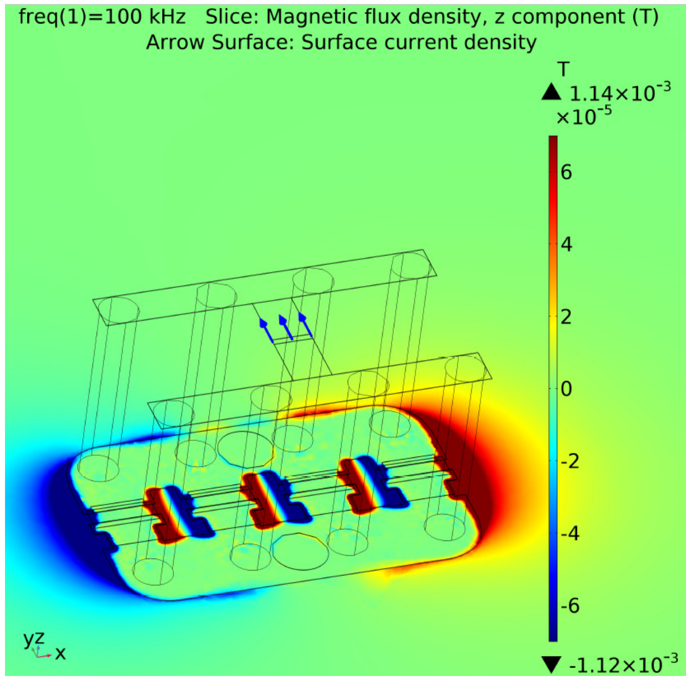

Figure 2.18: Magnetic field distribution of a fully balanced 4-die module

12.8 mV/A. Furthermore, it was also shown that the induced voltage is directly proportional to the input current amplitude as they have a linear relationship. Moreover, it is shown that for balanced current distribution between two paralleled GaN HEMTs dies, the detector picks up almost zero magnetic flux, except few nV of transient noise that could partially be due to simulation step size estimation as well. These studies also revealed that the magnetic flux density distribution is symmetrical for balanced conducting GaN dies, regardless of operating frequency, given a fully symmetrical layout and input port. Same set of simulations can be used to characterize the magnetic field distribution for various ON-resistance conditions in four-die and eight-die modules. One snapshot of a four-die simulation can be seen in Figure 2.18. These sort of simulations would be the initial step for the employment of the mismatch sensor, in order to improve system reliability.

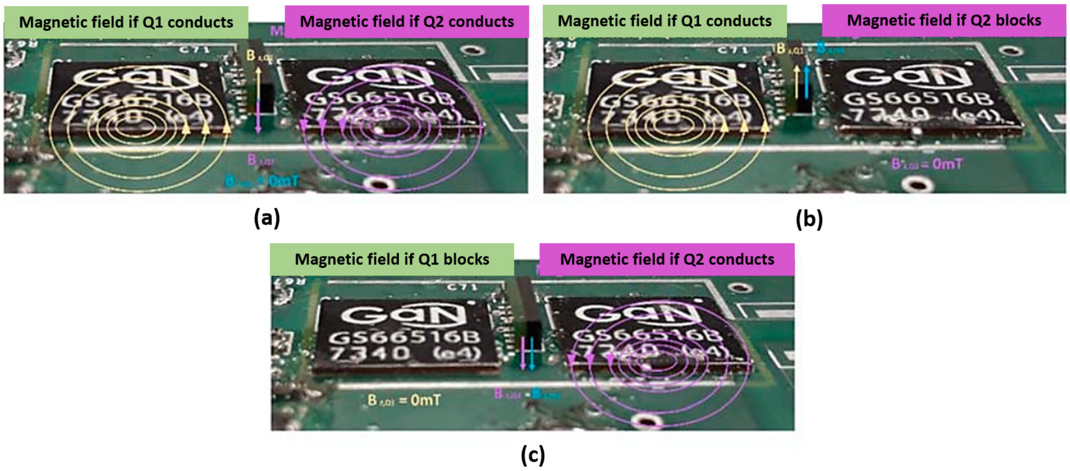

Figure 2.19: Simplified magnetic field distribution of a paralleled GaN pair [2], © 2019 IEEE.

2.4 Prototyped Designs and Experimental Results

Based on the characteristics of the GaN devices and the symmetric current sharing between them, a magnetic field with equal magnitude and the opposite direction is created around the two paralleled GaNs. This leads to destructive interference, as confirmed in magnetic field simulations. Given this, it was derived that the sensor output should be the same as the one without a current. Consequently, the sensor output voltage value during balanced conduction test is set as the reference for the current mismatch system.

Figure 2.19 (b) showcases a scenario where only the left-hand transistor Q1 conducts current, while Q2 is turned off, resulting in a current mismatch greater than zero. This creates a magnetic field greater than zero, reducing the output voltage and causing the sensor output voltage to drop. In contrast, Figure 2.19 (c) depicts the case where only Q2 conducts current, leading to an expected increase in the output voltage. These experimental variations are used to determine the sensitivity of the proposed current sensor [3].

As shown in Figure 2.20, a commercially available AMR sensor (HMC1051ZL, or HMC1041Z) is integrated as a current mismatch sensor between two paralleled GaN

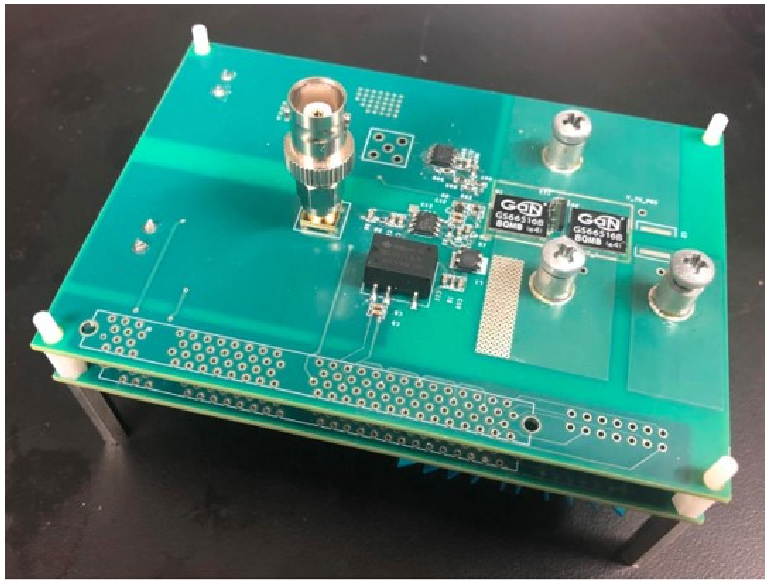

Figure 2.20: First prototype of a paralleled GaN buck converter, including an AMR mismatch current sensor.

HEMT devices (GS66516B). The test procedure includes three different stages:

- Measuring the AMR sensor output whilst both devices conduct current.
- Measuring the AMR sensor output whilst only Q1 conducts current.
- Measuring the AMR sensor output whilst only Q2 conducts current.

Using the proposed testing procedure, the current mismatch sensor was characterized under a different frequencies and current values. The results show an almost linear relationship between current mismatch and AMR sensor output.

Figure 2.21 demonstrates the sensor response for three different experimental scenarios. In Figure 2.21 (a), the sensor output remains constant due to both GaN devices carrying half of the switch current equally. Figure 2.21 (b) shows the results for the case when Q2 only carries the switch current, resulting in an increase in the sensor output value with switch current increase. Similarly, Figure 2.21 (c) demonstrates the case when only Q1 carries the switch current, resulting in a decrease in sensor output value with switch current increase, valid up to 20A. The results confirm the operation of the proposed current mismatch sensor up to 20A with a sensor sensitivity of 25mV/A. The current mismatch sensor frequency of operation is limited to its magneto-resistive element, given the sufficient bandwidth and slew rate of the processing elements [2, 3].

On a second testbed, a Rogowski coil detector is integrated with a GaN-based buck converter that was developed to match the EM simulations. Figure 2.22 shows the prototype. Initial evaluations showed the raw sensor's sensitivity to be 150mV/A. For a fully balanced current distribution, the spikes were in orders of a few mV. The coil mildly filtered output signal is depictred in Figure 2.23. As can be observed, this coil picks up negligible switching noise when both GaN devices conduct (Figure 2.23 (a)).

A third high-frequency 650V/120A GaN HEMT half-bridge module, which is also compatible with point-field detector integration without any compromise, was proposed and implemented based on EM studies. Figure 2.24 shows the half-bridge module. This half-bridge module consists of two paralleled GaN HEMTs per switching node, and each switching pair is integrated with one current mismatch detector. The current mismatch detector was prototyped and characterized for single GaN conduction per switching node in a boost converter setup. The full setup, including the designed gate-driver board and interfacing motherboard, can be seen in Figure 2.25. The sensor's performance in a boost converter operation was not satisfactory due to the excess of EMI/conductive noise present around the sensor at the switching node in this modular design. In order to mitigate this issue, a magnetic shield could be designed, as well as sensor EMI filtering for noise immunity.

2.5 Conclusion and Analysis

Modern power modules require high levels of protection and reliability to ensure their optimum performance. With the increasing use of wide-bandgap (WBG) devices, the importance of reliability has become even more significant due to their high-power density. Over the years, the industry has seen significant advancements

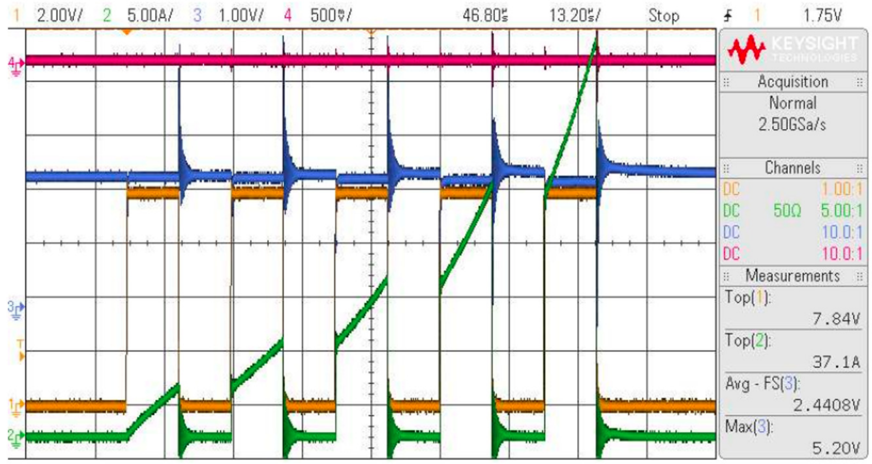

(a)

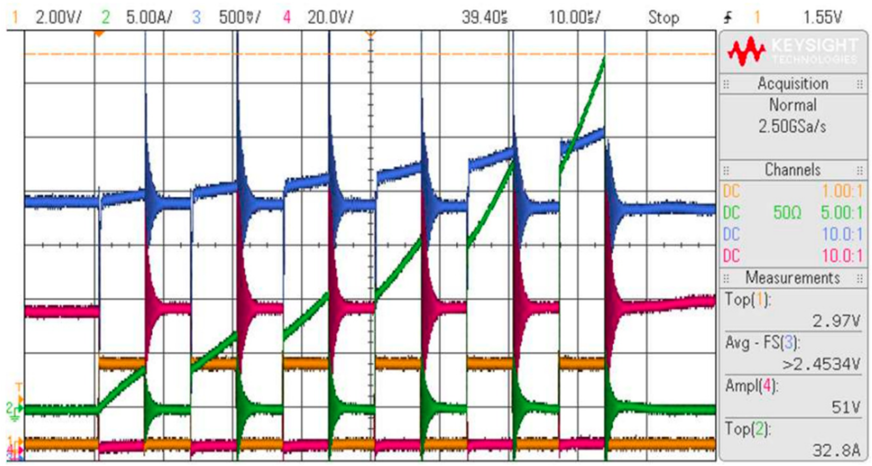

(b)

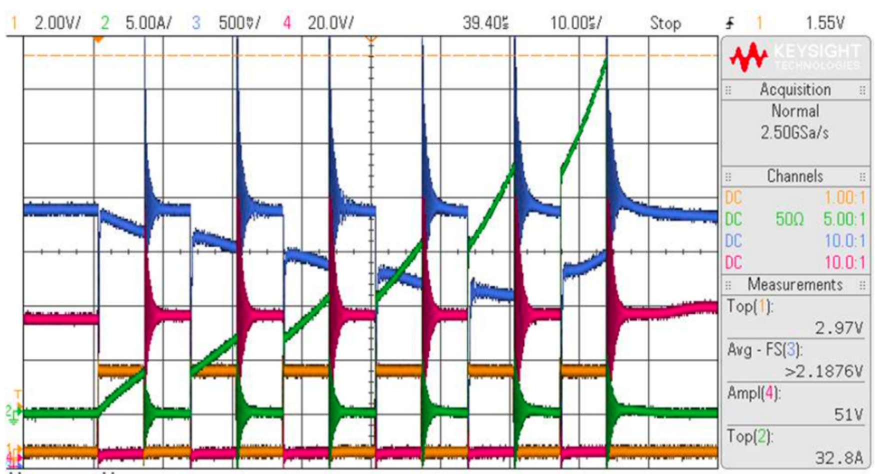

(c)

Figure 2.21: Multi-pulse measurement of the proposed AMR mismatch sensor. In (a), both devices are conducting. In (b), only Q2 is conducting. In (c), only Q1 is conducting. In all figures, green is the reference (total) switch-current measured by a 50A/50MHz current probe. Blue is the AMR mismatch current sensor output. Yellow is the PWM signal. Magenta is the switched voltage across the converter (this measurement wasn't recorded in Figure 2.21 (a) [3], © 2019 IEEE.

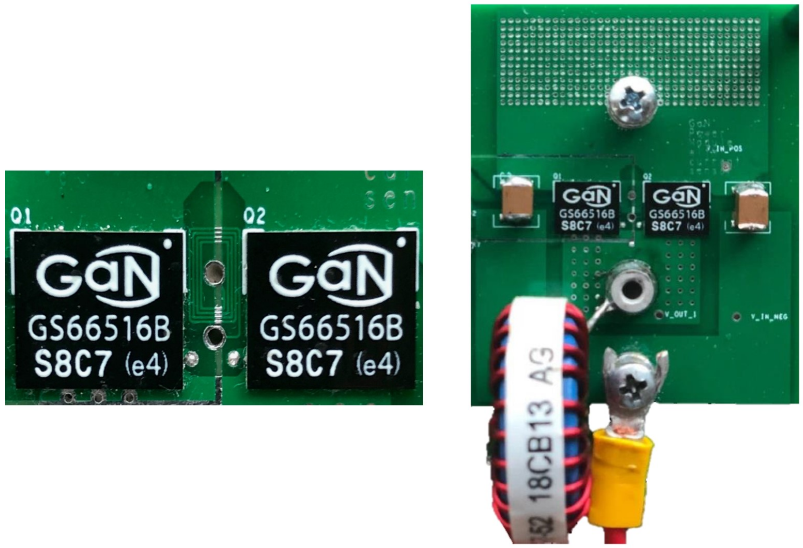

Figure 2.22: Prototyped paralleled GaN buck converter, including a coil as mismatch current sensor [3], © 2019 IEEE.

in current sensor technology, with single chip contactless sensors becoming more and more popular due to their efficiency and convenience. These sensors provide an excellent solution for the required measurements, and as such, they have been widely adopted across a range of power electronics applications. Monitoring power switches current sharing information is crucial to achieve reliable multichip power module designs. Therefore, a novel current mismatch sensor has been developed to measure the current difference between each pair of paralleled GaN devices .

Simulation studies have shown that there are spikes of only 67 nV during transients for fully balanced current distribution, which is very small, close to zero as expected from the theory. This indicates the neutral state, which is crucial for tuning the mismatch detector. Furthermore, simulations have shown that a single turn coil located in the specified area has a sensitivity of 12.7 mV/A based on EM simulations. The induced voltage has a direct linear relation with input current amplitude, as also confirmed by experiments that have shown the sensitivity of the prototyped detector to be around 150 mV/A.

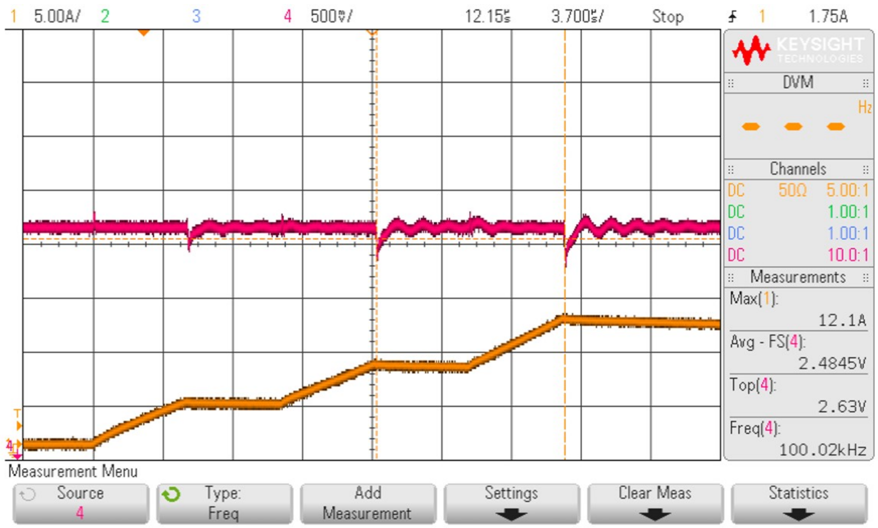

(a)

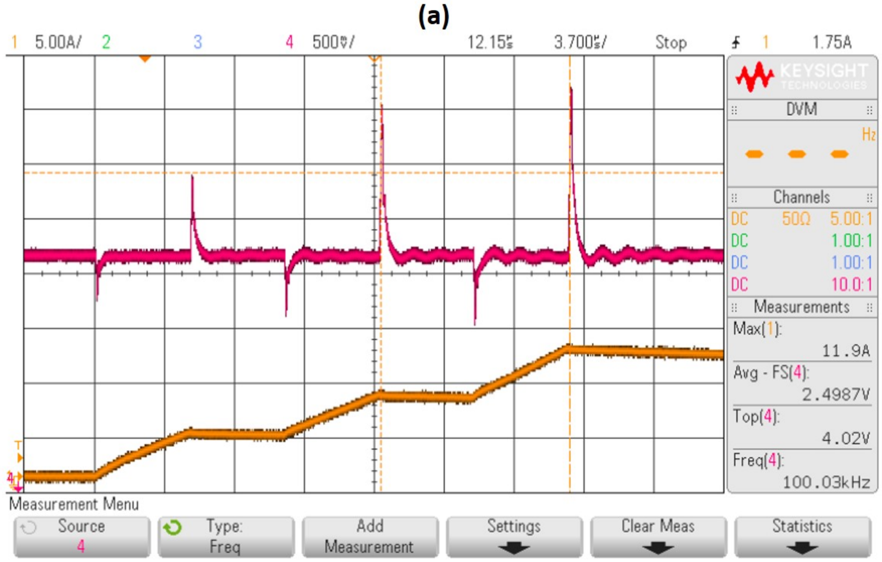

(b)

Figure 2.23: Multi-pulse measurement of the proposed coil mismatch sensor. In (a), both devices are conducting. In (b), only Q2 is conducting. In all figures, yellow is the reference load inductor current measured by a 50A/50MHz current probe. Magenta is the coil mismatch current sensor output [1], © 2020 IEEE.

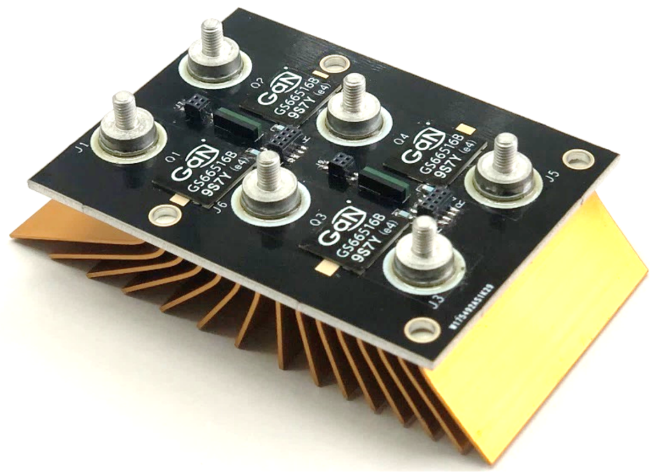

Figure 2.24: Prototyped GaN (GS66516B) half-bridge module, including AMR (HMC1051ZL) as the mismatch current sensor.

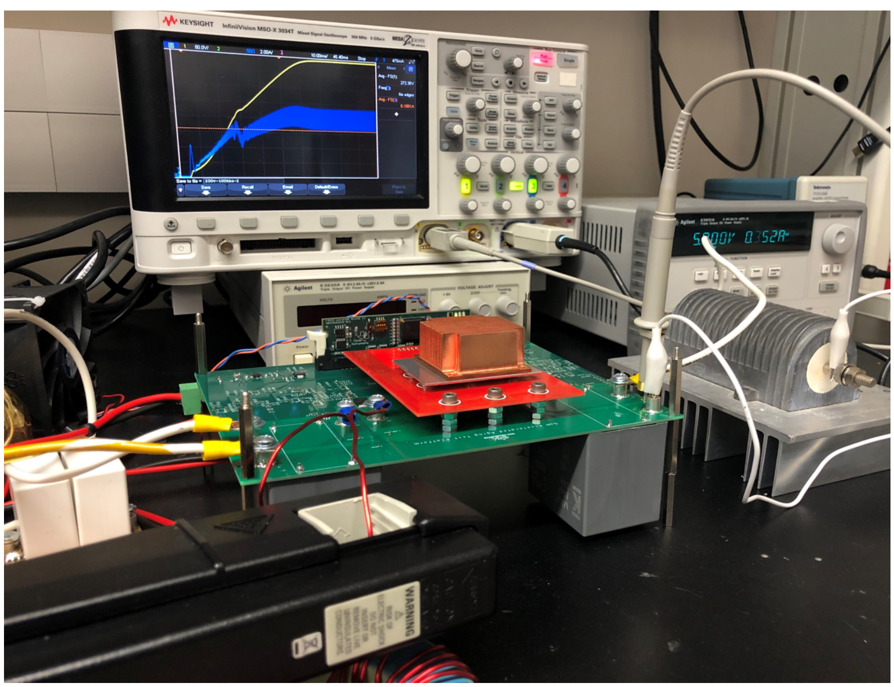

Figure 2.25: The boost converter setup for evaluation of the AMR mismatch sensor in the modular test bed design. The red PCB is the gate driver. The green PCB is the motherboard, including connections for input, load, and microcontroller. The silver plate on top of the red board is the half-bridge module shown in Figure 3.24. This specific capture is showing the boost concvrter stepping up a 200V to 400V. Blue waveform on the scope is the input current waveform measured with a 50 MHz current probe. Yellow is the load voltage measured with a 500 MHz passive probe.

Another sensing unit that has been experimentally verified to measure the current mismatch between two parallel GaN switches was an AMR detector. This unit can be applied for reliability assurance and circuit protection, among other purposes. Several measurements have been conducted, and the sensitivity has been determined to be approximately 25 mV/A. For calibration, it is recommended to utilize the case where both transistors are carrying the same current as a reference value. Experiments with various frequencies, as well as DC, have proved this hypothesis.

The analysis of the results affirms that lateral GaN devices carry current in 2-D, and as such, the assumption to determine the current mismatch by measuring the z-component of the magnetic field has been verified. The resultant data provided from the current mismatch sensor can be used for prognostic and protection purposes. This data is particularly useful for predicting device failure or protecting against short circuits, which can cause significant damage to the circuit or system.

The applications of the current mismatch sensor extend beyond its use in power electronics, and can be applied in an array of fields such as in; electric vehicles to detect the flow of current in the battery or to monitor the performance of the electric motor, as well as integrated into a variety of other systems, including renewable energy systems, data centers, and more.

A substantial advantage of the current mismatch sensor is its contactless nature, this eliminates the requirement of any physical connections to the system being measured. This makes it exemplary for use in harsh environments or situations where it may be difficult or impossible to make a physical connection. Additionally, the sensor has a small footprint, making it easy to integrate into a variety of systems.

Overall, reliability is a critical factor in achieving optimum performance for modern power modules. With the development of a novel current mismatch sensor, it is now possible to monitor power switches current sharing information, allowing for more reliable multichip power module designs. By providing an efficient and reliable solution for current sensing, this technology has the potential to significantly improve the performance and reliability of a range of systems, from power electronics to electric vehicles and beyond. With ongoing research and development, it is likely that the current mismatch sensor will continue to play an important role in the future of power electronics and other related fields. The simulations and experiments conducted have shown promising results, and future research will allow for a more in-depth analysis of the sensor's performance and characterization.

In future works, further analysis should be conducted on various point field detector performance for different current conduction modes. This will allow for a more comprehensive understanding of the current mismatch sensor's performance, and will aid in developing more reliable and efficient multichip power module designs.

CHAPTER 3: UNI-DIRECTIONAL RESET-LESS ROGOWSKI SWITCH CURRENT SENSOR

3.1 Background

Switch current measurement is a critical task required in many power electronics applicatoins such as, control, preditction, prognostics, protection, etc. There are various types of sensing technologies that could be exploited for such purpose. Amongts all, PCB-embedded Rogwski current sensors are very compact and low-cost, making the suitable to integrate with switching devices. Moreover, they could achieve a vary fast response, compared to other integrable magnetic field detectors. For the application of switch current measurement, researchers have used different approaches to compensate for lack of DC detection of Rogowski sensor, in order to take advantage of it's many great characteristics. Existing approaches are suitable, yet limiting for MHz operating frequency and high duty cycle applications. Hence, in this chapter, a novel compensation solution is proposed to correct the Rogowski sensor errors for unidirectional switching waveform measurement applications.

3.2 Rogowski Coil Design

In power electronics applications, particularly for switch current measurement, most of the frequency components of the switch current waveform are above the switching frequency up to dozens or hundreds of MHz, plus the DC value of the switching waveform. Therefore, a well-tuned ultrawide bandwidth sensor lacks only the DC component measurement. The inability to measure very low frequencies and DC causes droop in the measured current waveform, at the sensor's steady state condition. In this chapter, an analog compensator circuit is proposed to cancel the droop effect unidirectionally.

The Rogowski coil current sensor consists of three main components: a coil, a damping resistor (or termination resistor), and an integrator, as shown in Figure

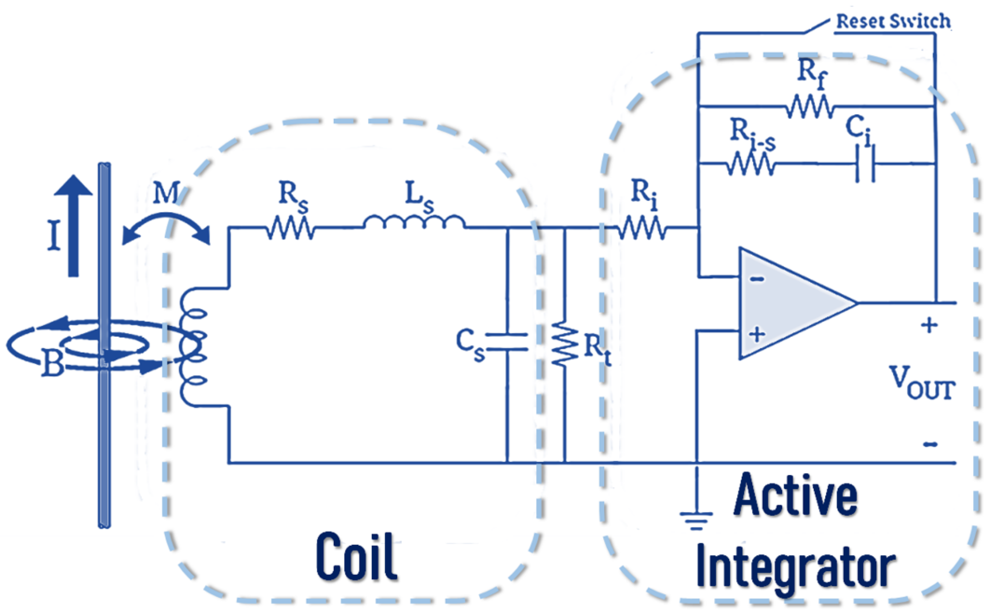

Figure 3.1: Simplified conventional Rogowski coil sensor schematic.

3.1. The figure also shows; the mutual inductance (M) between the coil and the current-carrying conductor, stray capacitance (C_s) of the coil, coil resistance (R_s), and self-inductance of the coil (L_s), with R_s being negligible for higher frequency analysis [77, 4].

By adding a terminating resistor (R_t), the coil will integrate from F_b to F_c, as depicted in Figure 3.2. To obtain the system's transfer function, the RC can be divided into its coil and integrator components. The complete transfer function of the coil model is given by equation (3.1).

$$\frac{V_{coil}(s)}{I(s)} = \frac{-MR_ts}{L_sR_tC_ss^2 + (R_sR_tC_s + L_s)s + R_s + R_t} \tag{3.1}$$

If the damping factor (R_t) is infinite, the Rogowski coil will have a double pole (or resonant frequency) at F_r, as expressed in equation (3.2).

$$F_r = \frac{1}{2\pi\sqrt{L_sC_s}} \tag{3.2}$$

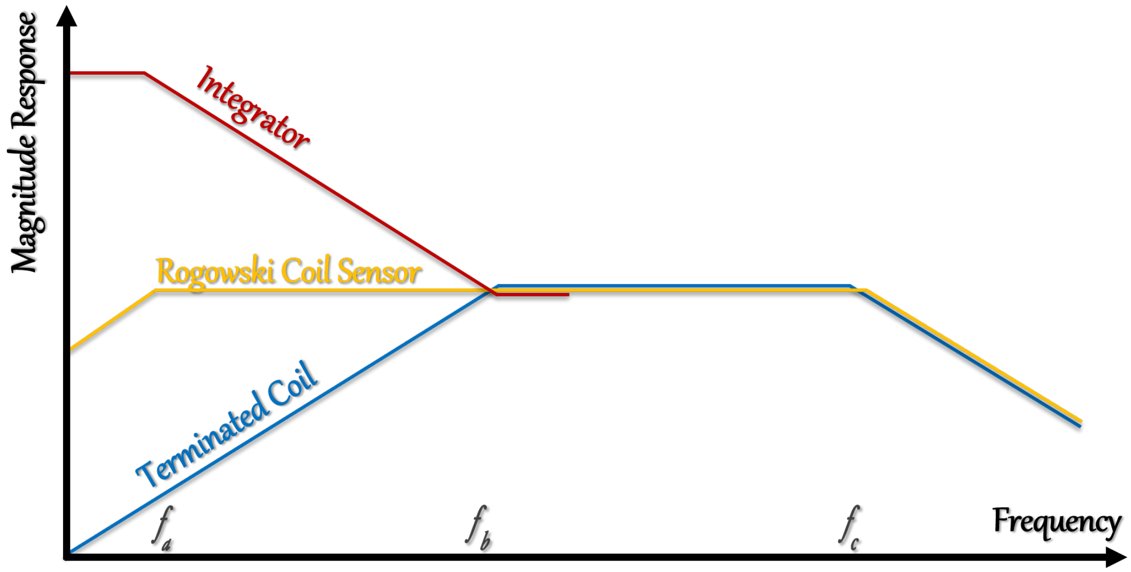

Figure 3.2: Theoritical magnitude response of a terminated coil, active integrator, and Rogowski coil sensor.

Therefore, a smaller value of R_t can split the double pole into two separate poles at F_b (for lower/medium frequencies) and F_c (for higher frequencies). The frequency range between these two poles is also known as the self-integrating bandwidth (BW) and over this frequency band, the coil output gain and phase responses remain almost constant, as indicated in reference [77]. Equations (3.3, 3.4) together with (3.1) can be used to approximate the self-integration gain and frequency of these two poles.

$$F_b = \frac{R_t + R_s}{2\pi L_s} \tag{3.3}$$

$$F_c = \frac{1}{2\pi R_t C_s} \tag{3.4}$$

Since the mutual inductance of an air-core coil is not significant enough, practical PCB-embedded coils cannot provide a constant gain below a few MHz, and an external integrator is required in order to compensate for the gain of the coil in frequencies before self-integration (F_b). That being said, a suitable choice in many cases is an analog op-amp-based integrator, due to its fast frequency response and relatively low cost. An inverting op-amp integrator can also be implemented to operate in the required frequency ranges with suitable gain and phase margins. An inverting analog integrator also provides higher stability measures due to its negative feedback topology. In Figure 3.1, R_i is the integrator resistance, C_i is the integrator capacitance, and R_{is} and R_f are the series resistance and negative feedback resistance, respectively. The transfer function of this inverting integrator is given in equation (3.5), with a single frequency pole set just before the starting of the integrating -20 dB/dec slope at the frequency of F_a (as shown in Figure 3.2).

$$\frac{V_{OUT}(s)}{V_{coil}(s)} = \frac{-R_f(R_{is}C_is + 1)}{R_i((R_{is} + R_f)C_is + 1)} \tag{3.5}$$

$$F_a = \frac{1}{2\pi(R_{is} + R_f)C_i} \tag{3.6}$$

The value of the integrator pole is determined by R_f, R_{is}, and C_i values. If these values are increased, the F_a will decrease. However, there are certain constraints to keep in mind:

- C_i cannot be set to a high value since it would lower the integrating factor and sensitivity of the sensor overall.
- R_{is} cannot have a large value as it is in series with the integrator capacitor.
- R_f is typically a finite value, even when set to open. This is due to the reason that practical opamps have internal feedback resistance to prevent saturation in DC or low frequencies.

Using given equations, the entire current sensor transfer function can be obtained (equation (3.7)). Inspecting equation (3.7), two zeros and three poles can be observed.

It can also be noted that one of the zeros is located at DC, meaning that this sensor has no DC response. In other words, it cannot detect DC components of the measured current.

$$\frac{V_{OUT}(s)}{I(s)} = \frac{MR_tR_f(R_{is}C_is+1)s}{R_i((R_{is}+R_f)C_is+1)(L_sR_tC_ss^2+(R_sR_tC_s+L_s)s+R_t+R_s)} \tag{3.7}$$

To fully utilize the sensor values and obtain a constant gain starting at frequency F_a up to F_c (as shown in Figure 3.2), one of the three poles (specifically the one in the middle) needs to be canceled out by the second zero of the transfer function. The role of R_{is} is to compensate for the phase leading of the capacitor at high frequencies. R_{is} creates a zero to match and cancel out the first coil's pole from equation (3.3) at the frequency of F_b (as shown in equations (3.8) and (3.9)).

$$F_b = \frac{1}{2\pi R_{is}C_i} = \frac{R_s+R_t}{2\pi L_s} \tag{3.8}$$

$$R_{is} = \frac{L_s}{(R_s+R_t)C_i} \tag{3.9}$$

Additionally, Figure 3.2 demonstrates that by intersecting the integrating slope of the integrator (-20 dB/dec) and the differentiating slope of the coil (+20 dB/dec), a persistent gain can be attained over an ultrawide frequency spectrum by tuning a large band of self-integration via the damping resistor.

The highest attainable bandwidth for the sensor using equations (3.1-3.9) can be from 10s of hertz (starting from F_a by setting a high enough R_f and C_i) and up to hundreds of MHz via low enough R_t and C_s (Figure 3.3) [77]. Having a large constant bandwidth directly influences the sensor's speed and accuracy.

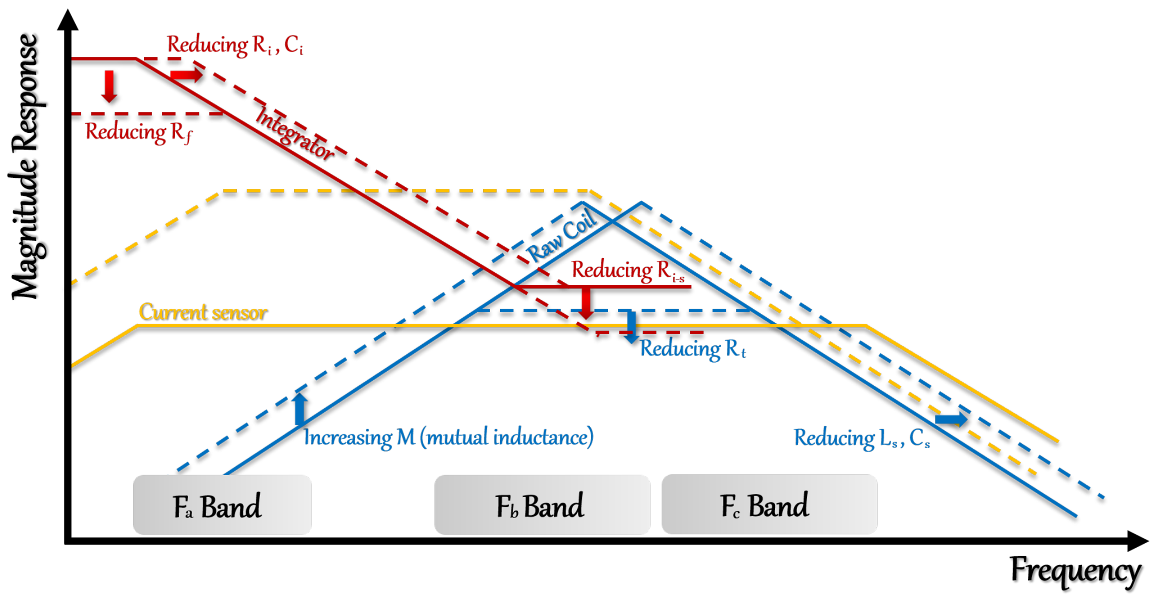

Figure 3.3: Wideband Rogowski coil comprehensive magnitude response plot.

3.3 The Novel Proccesing Circuit

The Rogowski coil current sensor is designed to measure the changing magnetic flux, and it requires an external processing circuit (integrator) to produce a proportional output. Matching the coil and integrator gains can result in a constant gain between the frequencies F_a and F_c, as shown in Figure 3.2. However, the lack of a DC response in the coil means that the integrator cannot reconstruct any DC components from the coil output voltage. Consequently, the integration of a measured zero value, results in an undetermined constant value, given an unknown initial value. Furthermore, the op-amp-based integrator suffers from input voltage/current offset non-idealities, which results in a DC offset error on the output.

Researchers have proposed different methods to compensate for the lack of DC measurement issues of a Rogowski coil current sensor. Two of the most used methodologies are:

- Resetting (discharging) the integrator capacitor consistently and in very short time frames

- Hybrid sensors: a combination of a Rogowski coil sensor and a DC detecting element such as Hall-effect/Magneto-resistor.

Using low-frequency sensors may seem attractive, but there are issues associated with deploying them in the switch current node, such as bulkiness, magnetic core saturation, and lack of EMI noise immunity.

That being said, the coil droop issue can be mitigated by discharging the integrator's capacitor synched complimentary with switch gate signals. This method is commonly used for switch-current measurements in medium-frequency converters. Nonetheless, the auxiliary reset circuit solution has the following major drawbacks:

- Impracticality for megahertz frequency and high-duty-cycle applications
- Inserts unwanted EMI/conductive noise on the sensor electronics
- Active circuit delay that needs to be compensated, limiting the maximum frequency of operation

To overcome these issues, the methodology used in this chapter combines the original AC-coupled Rogowski coil sensor (through a high-pass filter) with an inverting half-wave precision rectifier circuit, as shown in Figure 3.6.

The inverting half-wave rectifier (Figure 3.4) creates the inverse of the AC-coupled sensor's output during the off-cycle and zero during the on-state of the switch. The effectivness of variouse diode technologies is experimentally verified as shown in Figure 3.5. Table 3.1 describes the characteristics of different diodes used in this evaluation.

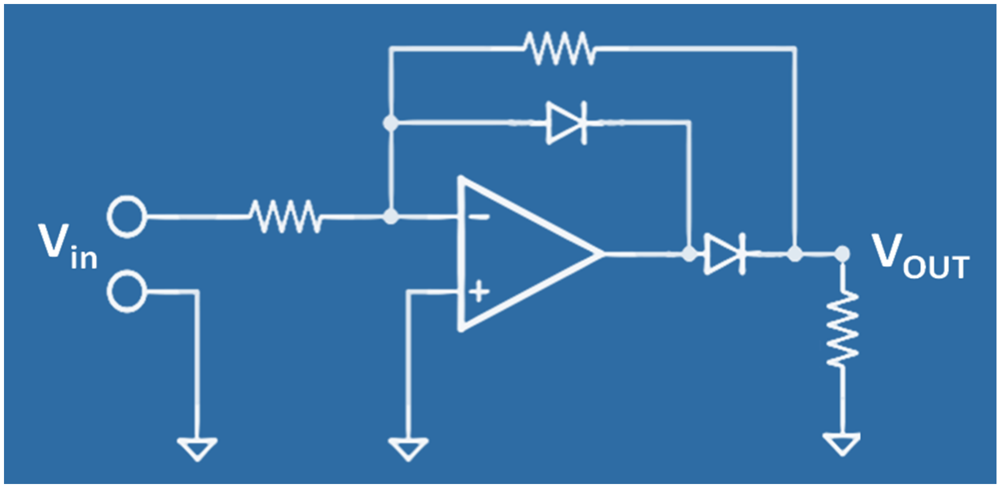

Figure 3.4: Wideband unidirectional Rogowski coil schematic, including the novel analog compensator circuit.

Table 3.1: Properties and characteristic response of four different diodes used to evalute the performance of the half-wave rectifier circuit.

Part Number	Capacitance	Response Delay @1MHz 100 mVpp (Period=1uS)	Response Delay @1MHz 1 Vpp (Period=1uS)
MEST2G-010-20	0.04 pF @10V 1MHz	NOT ENOUGH TIME TO RECOVER	200 nS
GMP4201-GM1	0.18 pF @10V 1MHz	NOT ENOUGH TIME TO RECOVER	300 nS
NSVRB751V40T1G	2.5 pF @1V 1MHz	300 nS	100 nS
1N4148W-E3-08	4 pF @0V 1MHz	500 nS	150 nS

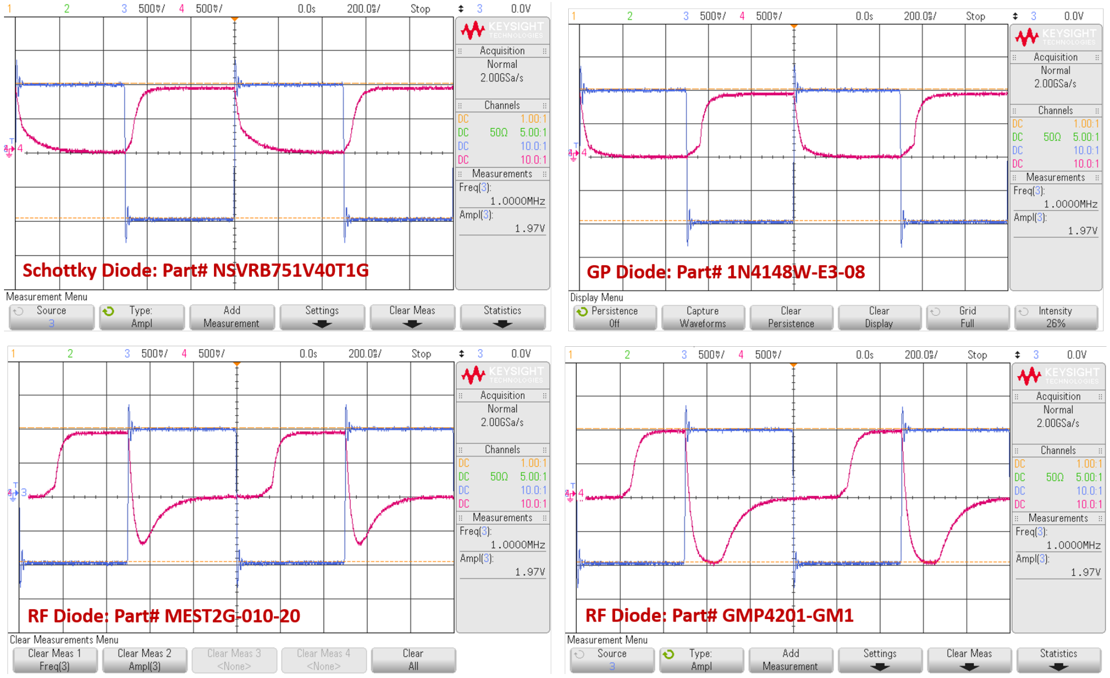

Figure 3.5: Precision half-wave rectifier performance using different diodes (circuit shown in figure 4.4). Blue is the input signal (-1V to +1V). Magenta is the half-wave rectifier output.

AC-coupled sensor output (thru high-pass filter) is intially connected as the input of the half-wave rectifier. Then, the AC-coupled sensor is fed forward to the output of the half-wave rectifier via R_{ff}. Value of R_{ff} was set to zero. Using this scheme, the diode circuit instantly eliminates the droop effect at every off-cycle, and the compensator does not allow the error to increase over time. This method works, solely due to the fact that the sensor output initially has no error and builds up over time. This is the exact same reason enabling the integrator discharge solution previously used in literature. The main advantage is that the compensator circuit does not require external controlling signal, while providing very fast response for ultra high-frequency signal measurement corrections. Frequency response analysis and simulations in MATLAB showed that adding the rectifier after the high-pass filter would not significantly change the gain and BW below hundreds of MHz.

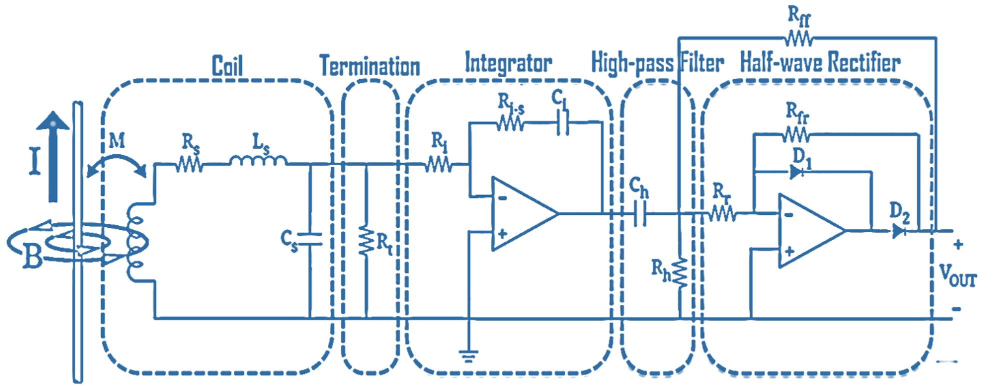

Figure 3.6: Unidirectional reset-less Rogowski sensor schematic, including the novel analog compensator circuit.

In summary, the Rogowski coil current sensor has limitations in measuring DC or extremely low-frequency components. Researchers have proposed different methods as compensation, including resetting the integrator and combining the Rogowski coil sensor with other DC detecting methods such as Hall-effect and MR. The methodology used in this paper combines the original AC-coupled RC with an inverting half-wave precision rectifier circuit, effectively eliminating the droop effect at every off-cycle instantly. As opposed to existing solutions, this method does not require external control, while a well designed coil could also be much more immune to unwanted surrounding EMIs.

3.4 Proposed Sensor Characteristics

The sensitivity and frequency response of a sensor are mainly influenced by the physical characteristics of the coil, as well as the values of the components shown in Figure 3.6. This figure depicts the equivalent circuit model of the coil, which consists of an inverting analog integrator as well as a high-pass filter. In order to calculate the sensor's sensitivity and gain a frequency response, all these sub-circuits must be taken into account.

In Figure 3.6, the mutual inductance, coil resistance, coil self-inductance, and coil stray capacitance are represented by M, R_s, L_s, and C_s, respectively. These values can be obtained theoretically by understanding the coil geometry and core material, which in this case, is air-core. Larger values of parasitic elements result in lower coil bandwidth. Therefore, there is a constant trade-off between a higher bandwidth boundary and a lower-band detection range for the coil.

The coil termination resistor, R_t, is known as the damping resistance. If the R_t is open, the coil will have a resonant frequency, F_r, as mentioned in equation (3.2). However, by reducing the value of R_t, the double pole at F_r can be transformed into two single poles at lower and higher frequencies, F_b and F_c, respectively. The coil will have a self-integrated output voltage between these two single poles and an integrator must be deployed to compensate for the increased gain of the coil for lower frequencies (F_a to F_b).

All in all, the physical characteristics of the coil and the values of its components, including M, R_s, L_s, C_s, and R_t significantly affect the sensor's sensitivity and its frequency response. The equivalent circuit model of the coil, consisting of an inverting analog integrator and a high-pass filter, must be considered to calculate the sensor's sensitivity and gain frequency response accurately. A larger value of parasitic elements reduces the coil bandwidth, resulting in a trade-off between higher bandwidth and lower-band detection scope for the coil. The coil termination resistor, R_t, plays a crucial role in determining the coil's resonant frequency and its self-integrated output voltage. To compensate for the increased gain of the coil at lower frequencies, an integrator needs to be deployed between F_a and F_b.

In this study, we examine the use of an AC-coupled Rogowski coil with a half-wave rectifier detector to measure the switching current in SiC high-current power modules. By shifting the zero average waveforms of the Rogowski coil up, we can maintain the DC value of the switch current artificially. More information on the formulation of the custom-designed coil can be found in [77].

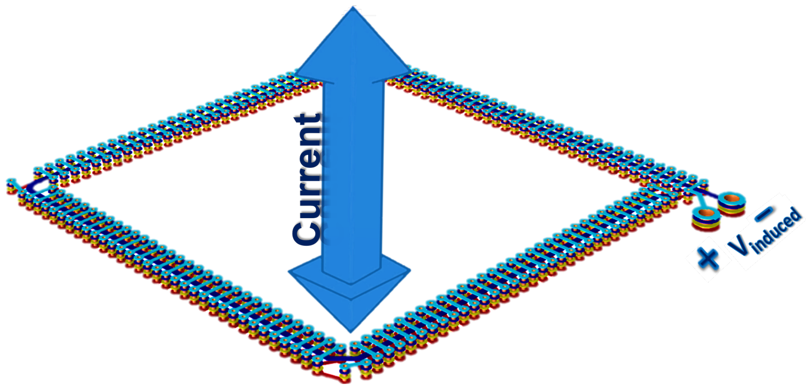

Figure 3.7: 3D view of the toroidal coil used for this work's prototype.

To demonstrate the effect of various parameters on the frequency response of the current sensor, a comprehensive Bode plot is provided in Figure 3.3. The alterations of each element can be studied in more detail in [77]. This design uses a toroidal PCB-embedded coil shown in Figure 3.7. The dimensions of the coil are 30 mm square edge side length, 3 mm coil trace width, and a PCB height of 2 mm. Figure 3.8 shows the prototyped unidirectional Rogowski switch current sensor.

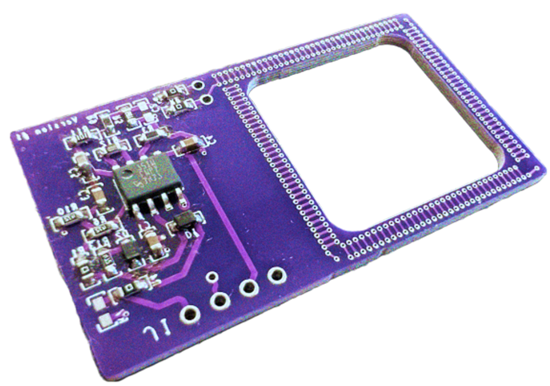

Figure 3.8: Prototyped unidirectional Rogowski coil sensor, including the novel analog compensator circuit [4], © 2023 IEEE.

To operate over a frequency range of 2 kHz up to hundreds of megahertz, the sensor is designed to have certain values and characteristics, as presented in Table 3.2, referring to the schematic shown in Figure 3.6. We have employed a high slew-rate voltage-feedback dual op-amp IC for this purpose (LM6172).

Table 3.2: Properties of the proposed Rogowski coil switch current sensor.

Property	Value
Number of Coil Turns	128
Mutual Inductance (M)	2.4 nH
Self-inductance (L_s)	540 nH
Stray Capacitance (C_s)	36 pF
Winding Resistance (R_s)	0.96 Ω
Termination Resistance (R_t)	6.80 Ω
Integrator Resistance (R_i)	36 Ω
Integrator Capacitance (C_i)	2 nF
Integrator Capacitance Series Resistance (R_is)	36 Ω
High-pass filter Capacitance (C_h)	100 nF
High-pass filter Resistance (R_h)	1 kΩ
Rectifier Input Resistance (R_r)	2 kΩ
Rectifier Feedback Resistance (R_fr)	2 kΩ
Rectifier Feedforward Resistance (R_ff)	1-5 Ω
Rectifier's Diode (D_1 and D_2)	300 mV Schottky
High-pass filter Cutoff Frequency (F_h)	1.6 kHz
Integrator Lower Band (F_a)	2 kHz
Self-integration Starting Frequency (F_b)	4 MHz
Sensor Highest Bandwidth (F_c)	340 MHz
Undampped Coil Resonant Frequency (F_r)	37 MHz
Overall Sensor Sensitivity	30 mV/A

In the next section, the performance of the sensor will be discussed, which has been tested over a wide range of switching frequencies and high-current operating conditions. The aim is to develop a highly accurate and reliable sensor that can measure the switching current in high-current WBG power modules. The proposed ultra-high bandwidth unidirectional reset-less topology can provide a significant improvement in terms of response time and accuracy compared to existing sensor designs.

3.5 Double Pulse Test (DPT) Experimental Results

To evaluate the detection accuracy of the low-band and demonstrate the large linear gain region, a series of double-pulse test (DPT) experiments have been conducted. As depicted in Figures 3.9, and 3.10, the sensor is able to accurately follow its reference signal for various currents and a shown maximum current of over 100A. Further confirmation of the sensor's linear gain range can be achieved with higher-current test setups utilizing appropriate reference probes. Since the coil used in this design does not have a magnetic core, it is able to provide a large linear gain range and has a high current capacity in general.

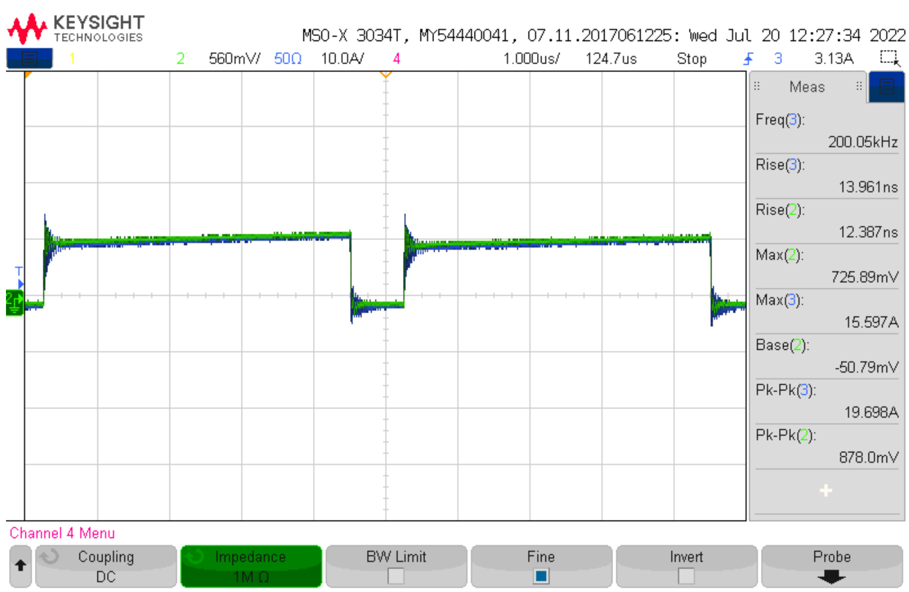

Figure 3.9: Double pulse test result, with equal pulse width of $500\mu s$ and duty cycle of %90. Blue is the proposed sensor output. Green is a reference 50A/50 MHz current probe.

Figure 3.10: Double pulse test result, with equal pulse width of 200μs and duty cycle of %60. Blue is the proposed sensor output. Green is a reference 50A/50MHz current probe.

Figure 3.11: Double pulse test result, with equal pulse width of 50μs and duty cycle of %85. Blue is the proposed sensor output. Green is a reference 50A/50MHz current probe.

The use of DPT experiments is crucial for evaluating the performance of the lower bandwidth of the sensor. By applying double pulses, we can evaluate the linearity and sensitivity of the sensor in a controlled setting. The results of the DPT experiments confirm that the sensor is able to accurately measure current over a wide range of values. The large linear gain range of the sensor is an important advantage of this design. It means that the sensor is able to provide accurate measurements even when reading very high currents and the linear gain range of the sensor can be further extended by increasing the number of turns in the coil. The air-core design of the coil allows avoiding the non-linearities and saturation effects that are often associated with a magnetic core. The lack of a magnetic core also means that the sensor is able to provide accurate measurements over a wide frequency range, while being compact and integrable.

3.6 DC-DC Converter Experimetnal Results

The experiment involves using a sensor to measure the current capture of a WBG DC-DC buck converter's top-device switch. The sensor has been specifically set up to capture a wide range of frequency components at the switching node.

The results of the experiment are displayed in Figure 3.12, which shows the start-up of the sensor compared to transient start-up of the converter. The graph indicates that the proposed sensor is capable of distinguishing a broad spectrum of frequency components at the switching node. Furthermore, the zoom-in capture (Figure 3.13) illustrates the precision of the sensor in capturing the 1 MHz switching signal while maintaining a very significant linear gain around 100 A current.

To confirm the accuracy and resolution of the sensor at lower current levels in higher frequencies, the experiment was carried out using a 50% duty cycle and load size, and the converter was operated at 0.5 MHz. The results of this experiment are shown in Figure 3.14, which indicates that signals with oscillating frequencies of about 30 MHz are captured by the sensor, which is faster than the 50 MHz current

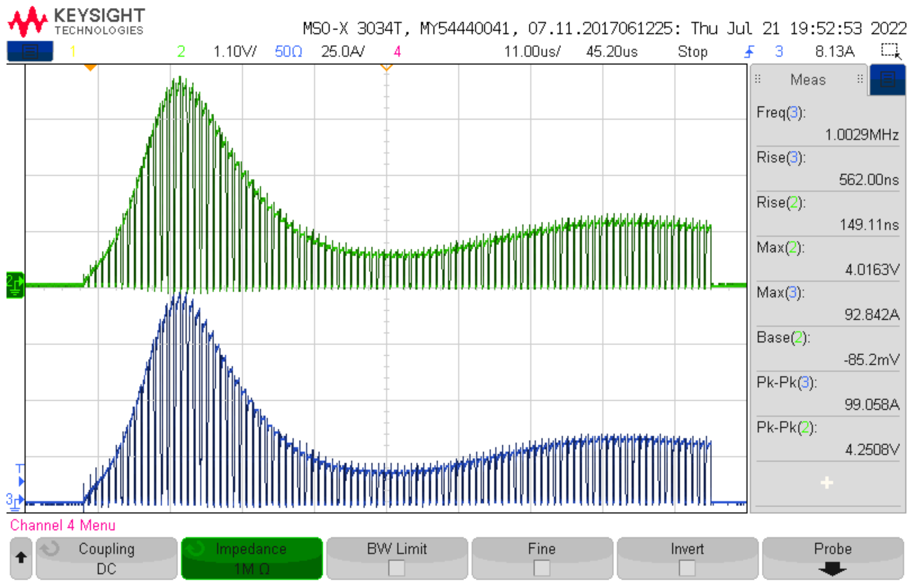

Figure 3.12: Buck converter switch current measurement results. Blue is the proposed sensor output. Green is the reference DC-50MHz current probe (TCP305A).

probe.

The sensor used in this experiment is designed to capture a wide range of frequency components at the switching moment. The switching frequency is an important parameter as it impacts the performance of the sensor. In this experiment, the switching frequency was set to 500 kHz, and the duty cycle was close to eighty percent, resulting in an off-state duration of less than 400 ns, which is a relatively short duration. However, the sensor was still able to capture signals with oscillating frequencies of about 30 MHz, which indicates its high precision and accuracy.

The results of this experiment demonstrate that the proposed sensor is capable of capturing a wide range of frequency components at the switching moment. The sensor is also able to maintain a very significant linear gain over 100 A current while the accuracy and resolution of the sensor are also confirmed at lower current levels in higher frequencies showing it can be used in a wide range of applications.

The sensor used in this experiment is capable of capturing a broad spectrum of frequency components at the switching moment. The experiment demonstrates that the

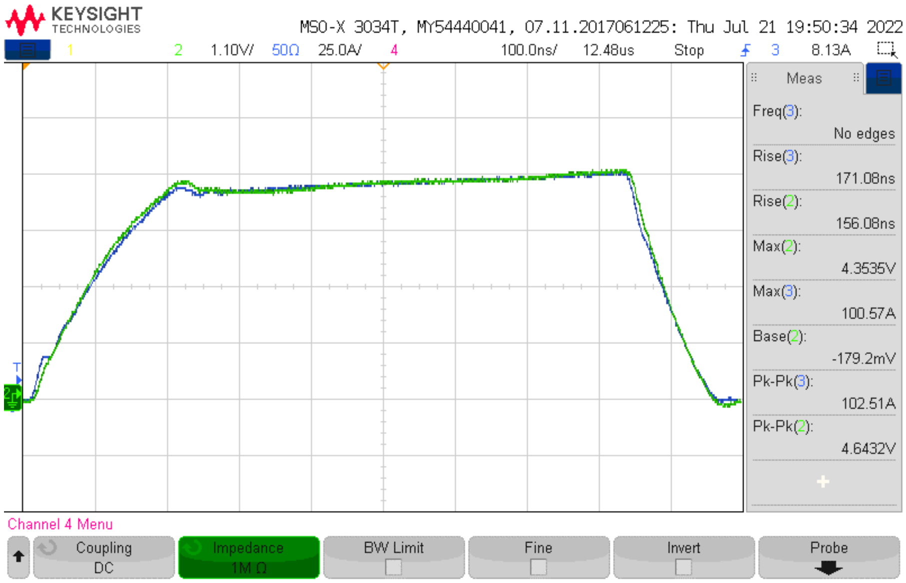

Figure 3.13: Buck converter switch current measurement results, with equal pulse width of 1μs and duty cycle of %85. Blue is the proposed sensor output. Green is a reference 50A/50MHz current probe.

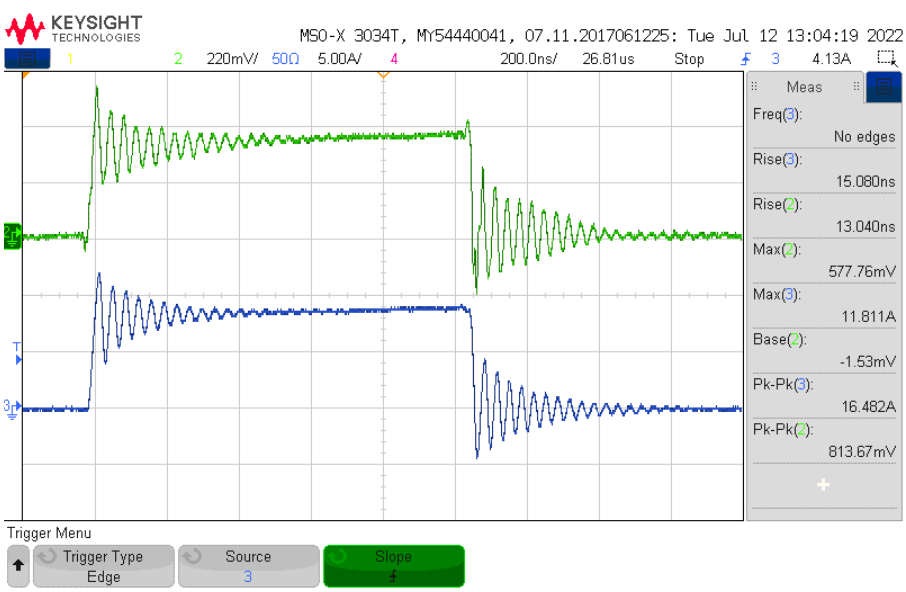

Figure 3.14: Buck converter switch current measurement results (zoomed-in).

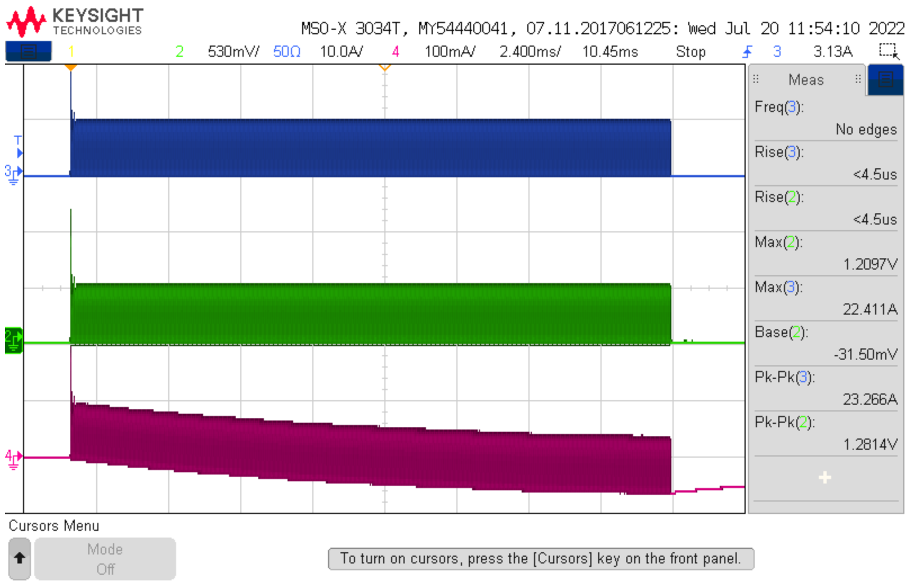

Figure 3.15: Long run (>1s) measurement of the SiC switch current. Blue is the proposed sensor output. Green is the reference DC-50MHz current probe (TCP305A). Magenta is the output of a secondary commercial 30 MHz Rogowski probe reference.

sensor is highly accurate, and precise even at low current levels in higher frequencies. The proposed sensor has significant potential for use in a variety of applications, and its high precision and accuracy make it a promising technology for future research and development.

3.7 Conclusion and Analysis

Figure 3.8 displays the PCB-embedded Rogowski coil switch current sensor that was fabricated on FR-4, with characteristics listed in Table 3.2. To validate the performance of the sensor, a high-frequency SiC half-bridge (s) test setup was employed. The final output of the sensor was measured using a 500 MHz passive probe, which was connected to a 350 MHz Keysight oscilloscope (MSO-X 3034T).

The experiment involved testing the sensor's performance under a range of switching frequencies and current amplitudes. The proposed topology was compared with a DC-50 MHz current probe (TCP305A) in order to confirm its functionality. The switch current waveforms, in most cases over 100A capture, consisted of a positive DC value, along with higher frequency elements starting from the switching frequency

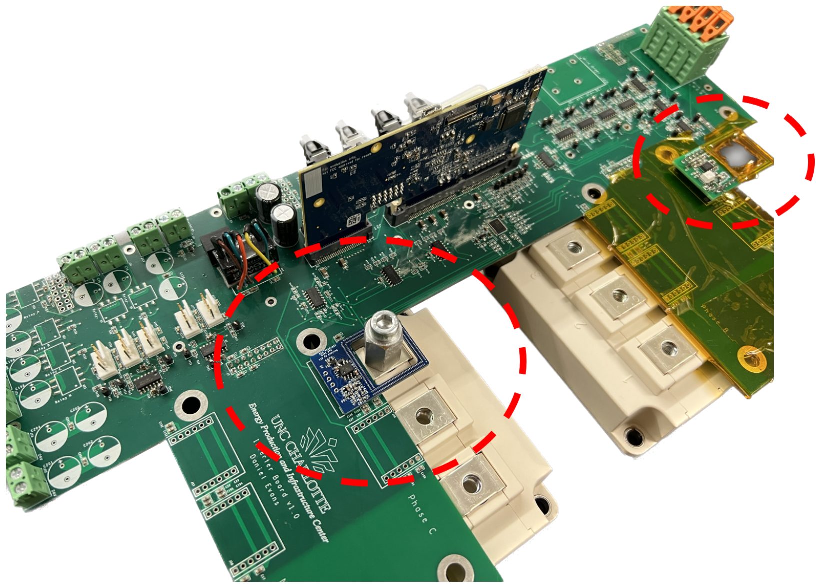

Figure 3.16: Example of integrating the proposed sensor with wide bandgap power modules (this is solely a graphical demonstration; inverter board is designed by Daniel Evans of EPIC, UNCC).

up to tens of MHz.

The sensor used in this experiment is a PCB-embedded Rogowski switch current sensor that was fabricated on FR-4. The sensor's characteristics are listed in Table 3.2. The sensor was designed to measure the switch current of a high-frequency SiC half-bridge (s) test setup. The final output of the sensor was measured using a 500 MHz passive probe, which was connected to a 350 MHz Keysight oscilloscope (MSO-X 3034T).

Overall, the experiment demonstrated the effectiveness of the proposed topology in measuring switch currents. The sensor's design and characteristics demonstrate its ability to be used in a wide range of applications, particularly in high-frequency unidirectional switch current measurements. The results of this experiment provide valuable insights into the sensor's capabilities and can serve as a basis for further research and development into the technology.

CHAPTER 4: CONCLUSIONS

Today, the power electronics industry is at its booming stage, enabling a wide prospect of technologies. Its reach extends across many industries such as energy infrastructure, power generation and distribution, electric transportation, and renewable energy. This pioneering sector provides the ability to effectively manage electric power while allowing for control, conversion, regulation, and protection in a wide range of applications. It is not feasible to imagine the levels of energy efficiency and control we have today without the available power electronics infrastructure that has been built over the past two decades. As such, the development of power electronics continues to be a crucial area of research and innovation, driving advancements in areas such as renewable energy, electric transportation, and smart grids.

Taking it one step deeper, current sensing is a paramount factor in power electronics, playing a fundamental role in maintaining safe and efficient operation/control of subsystems. Current sensing has been used and implemented in many power electronics systems such as motor drives and converters control, short-circuit and fault detection, as well as equipment's prognostics and remaining useful life prediction. High-accuracy current sensing is vital in applications where the precise amount of current needs to be measured, such as motor control, battery charging, and power supply regulation. Current sensing also allows for the optimization of power usage which leads to improved energy efficiency and reduced energy waste. On the other hand, without current sensing, power electronics systems wouldn't be able to detect overcurrent conditions, which can lead to system failure, overheating, and even fire hazards. Therefore, current sensing solutions continue to be a major research area of interest in power electronics.

In the application of prognostics/protection, current sensing solutions are able to provide the information needed to train various AI algorithms, as well as the protection schemes/topologies. This is a critical set of data that enables efficient maintenance and management of power electronics systems. With the use of advanced analytics and machine learning techniques, it is feasible to predict the future health of electronic components and systems, allowing for timely maintenance and repair. Moreover, protection is crucial because it enables the early detection and diagnosis of faults and failures in critical components such as power semiconductors, capacitors, and transformers. By monitoring the health of these components, prognostics can provide early warnings of potential system failures, preventing costly downtime and reducing maintenance costs. Moreover, prognostics help to optimize the performance and energy efficiency of power electronics systems by identifying potential issues and enabling proactive maintenance and repair. In this context, a novel current mismatch sensing topology is proposed, prototyped, and tested in Chapter 2. The current mismatch detector provides a new set of data containing information about the current difference of adjacent paralleled high-frequency semiconductors. This newly made available information could be used for protection and prognostics, unlocking new research avenues for semiconductors remaining useful life estimation. Various prototypes were designed using 650V GaN HEMT lateral devices to prove the concept with experiments. In two of the prototypes, an AMR sensor (HMC1051ZL) was employed as a current mismatch detector. In a lateral buck-converter, the concept was proven and the results were promising as shown in Chapter 3. A modular multilayer half-bridge module was then developed including an AMR current mismatch sensor. The AMR sensor output for the modular design was heavily distorted due to existing EMI/conductive noise from neighboring subcircuits. Consequently, another half-bridge design was investigated with the inclusion of an XY-axis PCB-embedded softly filtered Rogowski coil sensor. Yet again, the output of the Rogowski mismatch sensor provided the correct information that proves the proposed concept.

On the topic of control, and power management, switching device current information has always been an essential dataset. This set of information allows for simplified and precise control of many power converters. Moreover, the switch current information can be a key trigger point to allow for the detection of overcurrent conditions, which can lead to system failure, overheating, and potential safety hazards. Switch current sensors are also very much the principal components required for device characterization besides the voltage sensors. This is while the measurement of switch current is challenging due to the fast switching times and high $\frac{d_i}{d_t}/\frac{d_v}{d_t}$ involved in power electronics circuits. Therefore, it requires specialized measurement techniques and instrumentation, in order to accurately measure the current flow. Therefore, a novel low-cost uni-directional switch current sensor is proposed, prototyped, and tested in Chapter 3. This sensor is based on a PCB-embedded Rogowski coil, including an auxiliary sub-circuit that provides automatic drift/droop compensation measuring a unidirectional switch current waveform. The sensor was evaluated in a SiC DC-DC converter setup. The results show a detection upper bandwidth of over 32MHz, measuring the high-side current of a SiC device with switching frequencies up to 1MHz. This sensor is custom-made for many applications including but not limited to DC-DC converters control/protection scheme design, as well as device characterization setups (e.g. double pulse tester boards).

The immediate future works would be defined as the implementation of mismatch current sensors within high-frequency converters, including EMI/EMC sensor shielding, as well as online machine learning algorithms to provide real-time prognostics. Moreover, the uni-directional Rogowski sensor could be integrated within appropriate DC-DC converters to provide information for current mode control, as well as ultra-fast over-current detection.

REFERENCES

[1] H. Niakan, A. P. Sirat, and B. Parkhideh, "Current distribution monitoring of paralleled gan hemts," in *2020 IEEE Energy Conversion Congress and Exposition (ECCE)*, pp. 2865–2870, 2020.

[2] A. Lauer, H. Niakan, M. Hiller, and B. Parkhideh, "Investigation on non-invasive current mismatch measurement in paralleled gan hemts," in *2019 10th International Conference on Power Electronics and ECCE Asia (ICPE 2019 - ECCE Asia)*, pp. 899–904, 2019.

[3] H. Niakan and B. Parkhideh, "Implementation and characterization of point field detectors for current mismatch measurements in paralleled gan hemts," in *2019 IEEE 7th Workshop on Wide Bandgap Power Devices and Applications (WiPDA)*, pp. 310–313, 2019.

[4] H. Niakan, A. P. Sirat, and B. Parkhideh, "A novel reset-less rogowski switch-current sensor," *IEEE Transactions on Power Electronics*, vol. 38, no. 4, pp. 4203–4206, 2023.

[5] C. Xiao, L. Zhao, T. Asada, W. Odendaal, and J. van Wyk, "An overview of integratable current sensor technologies," in *38th IAS Annual Meeting on Conference Record of the Industry Applications Conference, 2003.*, vol. 2, pp. 1251–1258 vol.2, 2003.

[6] A. M. Patel and M. Ferdowsi, "Advanced current sensing techniques for power electronic converters," in *2007 IEEE Vehicle Power and Propulsion Conference*, pp. 524–530, 2007.

[7] H. Forghani-zadeh and G. Rincon-Mora, "Current-sensing techniques for dc-dc converters," in *The 2002 45th Midwest Symposium on Circuits and Systems, 2002. MWSCAS-2002.*, vol. 2, pp. II–II, 2002.

[8] D. Kim, "Phase current sensing technique for two-phase three-leg inverters using three shunt resistors," in *Journal of Power Electronics*, pp. 277–286, 2022.

[9] A. Patel and M. Ferdowsi, "Current sensing for automotive electronicsâa survey," *IEEE Transactions on Vehicular Technology*, vol. 58, no. 8, pp. 4108–4119, 2009.

[10] F. Rahmatian, "High-voltage current and voltage sensors for a smarter transmission grid and their use in live-line testing and calibration," in *IEEE PES General Meeting*, pp. 1–3, 2010.

[11] M. Biglarbegian, S. J. Nibir, H. Jafarian, and B. Parkhideh, "Development of current measurement techniques for high frequency power converters," in *2016 IEEE International Telecommunications Energy Conference (INTELEC)*, pp. 1–7, 2016.

[12] J. Wang, Z. Shen, R. Burgos, and D. Boroyevich, "Integrated switch current sensor for shortcircuit protection and current control of 1.7-kv sic mosfet modules," in *2016 IEEE Energy Conversion Congress and Exposition (ECCE)*, pp. 1–7, 2016.

[13] T. Funk and B. Wicht, "A fully integrated dc to 75 mhz current sensing circuit with on-chip rogowski coil," in *2018 IEEE Custom Integrated Circuits Conference (CICC)*, pp. 1–4, 2018.

[14] J. Wang, S. Mocevic, Y. Xu, C. DiMarino, R. Burgos, and D. Boroyevich, "A high-speed gate driver with pcb-embedded rogowski switch-current sensor for a 10 kv, 240 a, sic mosfet module," in *2018 IEEE Energy Conversion Congress and Exposition (ECCE)*, pp. 5489–5494, 2018.

[15] S. J. Nibir, M. Biglarbegian, and B. Parkhideh, "A non-invasive dc-10-mhz wideband current sensor for ultra-fast current sensing in high-frequency power electronic converters," *IEEE Transactions on Power Electronics*, vol. 34, no. 9, pp. 9095–9104, 2019.

[16] S. J. Nibir, S. Hauer, M. Biglarbegian, and B. Parkhideh, "Wideband contactless current sensing using hybrid magnetoresistor-rogowski sensor in high frequency power electronic converters," in *2018 IEEE Applied Power Electronics Conference and Exposition (APEC)*, pp. 904–908, 2018.

[17] S. Mocevic, J. Wang, R. Burgos, and D. Boroyevich, "Rogowski switch-current sensor self-calibration on enhanced gate driver for 10 kv sic mosfets," in *2021 IEEE 12th Energy Conversion Congress Exposition - Asia (ECCE-Asia)*, pp. 1420–1425, 2021.

[18] W. Kim, S. Luo, G.-Q. Lu, and K. D. Ngo, "Integrated current sensor using giant magneto resistive (gmr) field detector for planar power module," in *2013 Twenty-Eighth Annual IEEE Applied Power Electronics Conference and Exposition (APEC)*, pp. 2498–2505, 2013.

[19] S. Shao, N. Yu, X. Xu, J. Bai, X. Wu, and J. Zhang, "Tunnel magnetoresistance-based short-circuit and over-current protection for igbt module," *IEEE Transactions on Power Electronics*, vol. 35, no. 10, pp. 10930–10944, 2020.

[20] Y. Feng, S. Shao, J. Du, Q. Chen, J. Zhang, and X. Wu, "Short-circuit and over-current fault detection for sic mosfet modules based on tunnel magnetoresistance with predictive capabilities," *IEEE Transactions on Power Electronics*, vol. 37, no. 4, pp. 3719–3723, 2022.

[21] S. Mocevic, J. Wang, R. Burgos, D. Boroyevich, M. Jaksic, M. Teimor, and B. Peaslee, "Phase current sensor and short-circuit detection based on rogowski coils integrated on gate driver for 1.2 kv sic mosfet half-bridge module," in *2018 IEEE Energy Conversion Congress and Exposition (ECCE)*, pp. 393–400, 2018.

[22] H. Givi, “Switch fault diagnosis and capacitor lifetime monitoring technique for dcâdc converters using a single sensor,” *IET Science, Measurement Technology*, vol. 10, no. 5, pp. 513–527, 2016.

[23] C. Roy, N. Kim, H. Niakan, A. Parsa Sirat, and B. Parkhideh, “An ultra-fast and non-invasive short circuit protection strategy for a wbg power electronics converter with multiple half-bridge legs,” in *2020 IEEE Energy Conversion Congress and Exposition (ECCE)*, pp. 2505–2510, 2020.

[24] E. Farjah, H. Givi, and T. Ghanbari, “Application of an efficient rogowski coil sensor for switch fault diagnosis and capacitor esr monitoring in nonisolated single-switch dcâdc converters,” *IEEE Transactions on Power Electronics*, vol. 32, no. 2, pp. 1442–1456, 2017.

[25] H. Yoon and Y. Cho, “Application of the rogowski coil current sensor for over-current detection and blocking in power conversion systems,” in *2019 10th International Conference on Power Electronics and ECCE Asia (ICPE 2019 - ECCE Asia)*, pp. 1–7, 2019.

[26] F. Erturk, E. Ugur, J. Olson, and B. Akin, “Real-time aging detection of sic mosfets,” *IEEE Transactions on Industry Applications*, vol. 55, no. 1, pp. 600–609, 2019.

[27] M. Tsukuda, M. Koga, K. Nakashima, and I. Omura, “Micro pcb rogowski coil for current monitoring and protection of high voltage power modules,” *Microelectronics Reliability*, vol. 64, pp. 479–483, 2016.

[28] Z. Z. Z. X. Jiao C, Zhang Z, “Integrated rogowski coil sensor for press-pack insulated gate bipolar transistor chips,” *Sensors*, vol. 20, no. 15, p. 4080, 2020.

[29] Y. Xue, J. Lu, Z. Wang, L. M. Tolbert, B. J. Blalock, and F. Wang, “A compact planar rogowski coil current sensor for active current balancing of parallel-connected silicon carbide mosfets,” in *2014 IEEE Energy Conversion Congress and Exposition (ECCE)*, pp. 4685–4690, 2014.

[30] H. Li, S. Beczkowski, S. Munk-Nielsen, K. Lu, and Q. Wu, “Current measurement method for characterization of fast switching power semiconductors with silicon steel current transformer,” in *2015 IEEE Applied Power Electronics Conference and Exposition (APEC)*, pp. 2527–2531, 2015.

[31] D. Braun, R. Lukaszewski, D. Pixler, and G. Skibinski, “Use of a co-axial ct and planar bus to improve igbt device characterization,” in *IAS ’96. Conference Record of the 1996 IEEE Industry Applications Conference Thirty-First IAS Annual Meeting*, vol. 3, pp. 1507–1516 vol.3, 1996.

[32] P. Poulichet, F. Costa, and E. Laboure, “A new high-current large-bandwidth dc active current probe for power electronics measurements,” *IEEE Transactions on Industrial Electronics*, vol. 52, no. 1, pp. 243–254, 2005.

[33] L. Shillaber, L. Ran, Y. Shen, and T. Long, "Gigahertz current measurement for wide band-gap devices," in *2020 IEEE Energy Conversion Congress and Exposition (ECCE)*, pp. 2357–2363, 2020.

[34] G. Han, M. Wu, Z. Lu, W. Liu, and B. Zhu, "Phase current measurement method for switched reluctance motors with one current sensor," *IEEE Transactions on Transportation Electrification*, vol. 9, no. 1, pp. 699–711, 2023.

[35] H. Yan, Y. Xu, W. Zhao, H. Zhang, and C. Gerada, "Dc drift error mitigation method for three-phase current reconstruction with single hall current sensor," *IEEE Transactions on Magnetics*, vol. 55, no. 2, pp. 1–4, 2019.

[36] C. Gan, J. Wu, N. Wang, Y. Hu, W. Cao, and S. Yang, "Independent current control of dual parallel srm drive using a public current sensor," *IEEE/ASME Transactions on Mechatronics*, vol. 22, no. 1, pp. 392–401, 2017.

[37] H. Yan, W. Wang, Y. Xu, and J. Zou, "Position sensorless control for pmsm drives with single current sensor," *IEEE Transactions on Industrial Electronics*, vol. 70, no. 1, pp. 178–188, 2023.

[38] Y. Zhang, W. Lu, J. Guo, Y. Zhang, Z. Chen, Y. Zhang, and L. Ji, "A novel on-chip cmos current sensor implemented by switched capacitors for a current-mode control dc-dc buck converter," in *2011 IEEE International Conference of Electron Devices and Solid-State Circuits*, pp. 1–2, 2011.

[39] M. Du and H. Lee, "A 2.5mhz, 97dynamically-biased shunt feedback for current-mode switching dc-dc converters," in *2008 IEEE International Symposium on Circuits and Systems (ISCAS)*, pp. 3274–3277, 2008.

[40] H. Wang, X. Hu, Q. Liu, G. Zhao, and D. Luo, "A novel on-chip current-sensing structure for current-mode dc-dc converter," in *2013 International Symposium onVLSI Design, Automation, and Test (VLSI-DAT)*, pp. 1–4, 2013.

[41] S. Singh, D. Mandal, B. Bakkaloglu, and S. Kiaei, "Low-power/low-voltage integrated cmos sense resistor-free analog power/current sensor compatible with high-voltage switching dcâdc converter," *IEEE Transactions on Circuits and Systems I: Regular Papers*, vol. 66, no. 6, pp. 2208–2218, 2019.

[42] T. Funk and B. Wicht, "A fully integrated dc to 75 mhz current sensing circuit with on-chip rogowski coil," in *2018 IEEE Custom Integrated Circuits Conference (CICC)*, pp. 1–4, 2018.

[43] T. E. D. Kizas, M. Bergo, G. Capodivacca, L. Scandola, P. Malcovati, and A. Baschirotto, "A 51-ns response-time, fully integrated, high-side current sensor for a 40-v 6-a dcâdc converter," *IEEE Solid-State Circuits Letters*, vol. 5, pp. 300–303, 2022.

[44] V. Gogolou, T. Laopoulos, and S. Siskos, "A wide range current sensing technique for integrated dc-dc converters," in *2022 37th Conference on Design of Circuits and Integrated Circuits (DCIS)*, pp. 01–04, 2022.

[45] W. Chen, C. Yang, L. Chen, and P. Gui, "A 2mhz 4-48v V_{in} flying-capacitor based floating-ground gan dc-dc converter with real-time inductor peak-current detection and 6μs load transient response," in *2022 IEEE Radio Frequency Integrated Circuits Symposium (RFIC)*, pp. 151–154, 2022.

[46] B. M. S. R. D. A. Chojowski, M., "High-frequency current transformers cascade for power electronics measurements," *Sensors*, vol. 15, no. 22, p. 5846, 2022.

[47] S. Yin, Y. Wu, M. Dong, J. Lin, and H. Li, "Design of current transformer for in situ current measurement of discrete sic power devices," *IEEE Journal of Emerging and Selected Topics in Industrial Electronics*, vol. 3, no. 4, pp. 1077–1086, 2022.

[48] M. Sheng, M. H. Alvi, and R. D. Lorenz, "20 mhz integrated current sensing for wbg systems with emi suppression," in *2018 IEEE Energy Conversion Congress and Exposition (ECCE)*, pp. 375–382, 2018.

[49] J. N. Fritz, C. Neeb, and R. W. De Doncker, "A pcb integrated differential rogowski coil for non-intrusive current measurement featuring high bandwidth and dv/dt immunity," in *Power and Energy Student Summit(PESS) 2015*, 2015.

[50] S. Ranasingh, T. Pradhan, and D. K. Raju, "Contactless current sensor with novel coil designs and hall-effect based electron device for dynamic precision adjustment," *IEEE Sensors Journal*, vol. 22, no. 21, pp. 20626–20634, 2022.

[51] P. S. Niklaus, D. Bortis, and J. W. Kolar, "High-bandwidth high-cmrr current measurement for a 4.8 mhz multi-level gan inverter ac power source," in *2021 IEEE Applied Power Electronics Conference and Exposition (APEC)*, pp. 200–207, 2021.

[52] P. S. Niklaus, D. Bortis, and J. W. Kolar, "Beyond 50 mhz bandwidth extension of commercial dc-current measurement sensors with ultra-compact pcb-integrated pickup coils," *IEEE Transactions on Industry Applications*, vol. 58, no. 4, pp. 5026–5041, 2022.

[53] D. Koch, H. Bantle, J. Acuna, P. Ziegler, and I. Kallfass, "Design methodology for ultra-compact rogowski coils for current sensing in low-voltage high-current gan based dc/dc-converters," in *2021 23rd European Conference on Power Electronics and Applications (EPE'21 ECCE Europe)*, pp. P.1–P.9, 2021.

[54] H.-C. Chen, C.-Y. Lu, and C.-H. Lu, "Control of bidirectional interleaved dc-dc converter with single current sensor," in *2018 IEEE Energy Conversion Congress and Exposition (ECCE)*, pp. 2171–2177, 2018.

[55] M. S. Zaman, W. L. Jiang, S. Murray, H. De Vleeschouwer, P. Moens, J. Roig, and O. Trescases, "Integrated sensehemt and gate-driver on a 650-v gan-on-si platform demonstrated in a bridgeless totem-pole pfc converter," in *2020 32nd International Symposium on Power Semiconductor Devices and ICs (ISPSD)*, pp. 26–29, 2020.

[56] X. Zhao, R. Phukan, C.-W. Chang, D. Dong, R. Burgos, A. PLAT, and D. Mustapha, "Design of rogowski coil current sensor integrated with busbar and gate driver for 211 kw sic-based three-level t-type inverter," in *2022 IEEE Energy Conversion Congress and Exposition (ECCE)*, pp. 1–7, 2022.

[57] X. Zhao, R. Puhkan, C.-W. Chang, R. Burgos, P. Asfaux, S. Uicich, and D. Dong, "Design of ultra-compact gate driver integrated with current sensor and commutation path for a 211-kw three-level sic aircraft propulsion inverter," *IEEE Journal of Emerging and Selected Topics in Power Electronics*, pp. 1–1, 2023.

[58] W. Kim, S. Luo, G.-Q. Lu, and K. D. Ngo, "Integrated current sensor using giant magneto resistive (gmr) field detector for planar power module," in *2013 Twenty-Eighth Annual IEEE Applied Power Electronics Conference and Exposition (APEC)*, pp. 2498–2505, 2013.

[59] J. Wang, Z. Shen, C. DiMarino, R. Burgos, and D. Boroyevich, "Gate driver design for 1.7kv sic mosfet module with rogowski current sensor for shortcircuit protection," in *2016 IEEE Applied Power Electronics Conference and Exposition (APEC)*, pp. 516–523, 2016.

[60] J. Wang, Z. Shen, R. Burgos, and D. Boroyevich, "Design of a high-bandwidth rogowski current sensor for gate-drive shortcircuit protection of 1.7 kv sic mosfet power modules," in *2015 IEEE 3rd Workshop on Wide Bandgap Power Devices and Applications (WiPDA)*, pp. 104–107, 2015.

[61] U.-J. Kim, M. S. Song, and R. Y. Kim, "Pcb-based current sensor design for sensing switch current of a nonmodular gan power semiconductor," *Energies*, vol. 13, no. 19, p. 5161, 2020.

[62] J. Wang, Z. Shen, R. Burgos, and D. Boroyevich, "Integrated switch current sensor for shortcircuit protection and current control of 1.7-kv sic mosfet modules," in *2016 IEEE Energy Conversion Congress and Exposition (ECCE)*, pp. 1–7, 2016.

[63] Z. Zhou, Z. Xin, Q. Liu, and C. Li, "A differential compensated air coil current sensor for switching current measurement of power devices," *IEEE Transactions on Industrial Electronics*, vol. 70, no. 5, pp. 5356–5364, 2023.

[64] K. Wang, X. Yang, H. Li, L. Wang, and P. Jain, "A high-bandwidth integrated current measurement for detecting switching current of fast gan devices," *IEEE Transactions on Power Electronics*, vol. 33, no. 7, pp. 6199–6210, 2018.

[65] "Ieee standard computer dictionary: A compilation of ieee standard computer glossaries," *IEEE Std 610*, pp. 205–206, 1991.

[66] B. Lu and S. K. Sharma, "A literature review of igbt fault diagnostic and protection methods for power inverters," *IEEE Transactions on Industry Applications*, vol. 45, no. 5, pp. 1770–1777, 2009.

[67] M. L. Alghaythi, R. M. O'Connell, N. E. Islam, and J. M. Guerrero, "A multiphase-interleaved high step-up dc-dc boost converter with voltage multiplier and reduced voltage stress on semiconductors for renewable energy systems," in *2020 IEEE Power Energy Society Innovative Smart Grid Technologies Conference (ISGT)*, pp. 1–5, 2020.

[68] M. Oinonen, M. Laitinen, and J. KyyrÃ€, "Current measurement and short-circuit protection of an igbt based on module parasitics," in *2014 16th European Conference on Power Electronics and Applications*, pp. 1–9, 2014.

[69] A. V. Rocha, D. F. Melo, T. A. Carvalho Maia, V. N. Ferreira, and B. J. Cardoso Filho, "Iot-based degradation management for self-healing power converters," in *2019 IEEE Applied Power Electronics Conference and Exposition (APEC)*, pp. 2802–2809, 2019.

[70] Z. Zeng, X. Zhang, and X. Li, "Layout-dominated dynamic current imbalance in multichip power module: Mechanism modeling and comparative evaluation," *IEEE Transactions on Power Electronics*, vol. 34, no. 11, pp. 11199–11214, 2019.

[71] W. W. Z. NuTech Ventures Inc, Qiao and L. Qu, "Monitoring aging of power semiconductor devices based on case temperature," May 2019.

[72] L. T. M. Rockwell Automation Technologies Inc, Wei and R. Lukaszewski, "Power electronic module igbt protection method and system," April 2012.

[73] S. Mocevic, J. Wang, R. Burgos, D. Boroyevich, M. Jaksic, M. Teimor, and B. Peaslee, "Phase current reconstruction based on rogowski coils integrated on gate driver of sic mosfet half-bridge module for continuous and discontinuous pwm inverter applications," in *2019 IEEE Applied Power Electronics Conference and Exposition (APEC)*, pp. 1029–1036, 2019.

[74] C. Zhao, L. Wang, F. Zhang, and F. Yang, "A method to balance dynamic current of paralleled sic mosfets with kelvin connection based on response surface model and nonlinear optimization," *IEEE Transactions on Power Electronics*, vol. 36, no. 2, pp. 2068–2079, 2021.

[75] U. K. Mishra and M. Guidry, *Lateral GaN Devices for Power Applications (from kHz to GHz)*. Springer International Publishing.

[76] C. Zhao, L. Wang, and F. Zhang, "Effect of asymmetric layout and unequal junction temperature on current sharing of paralleled sic mosfets with kelvin-source connection," *IEEE Transactions on Power Electronics*, vol. 35, no. 7, pp. 7392–7404, 2020.

[77] A. P. Sirat, H. Niakan, C. Roy, and B. Parkhideh, "Rogowski-pair sensor for high-speed switch current measurements without reset requirement," in *2022 IEEE Energy Conversion Congress and Exposition (ECCE)*, pp. 1–8, 2022.

APPENDIX A: EXTRA FIGURES AND CAPTURES

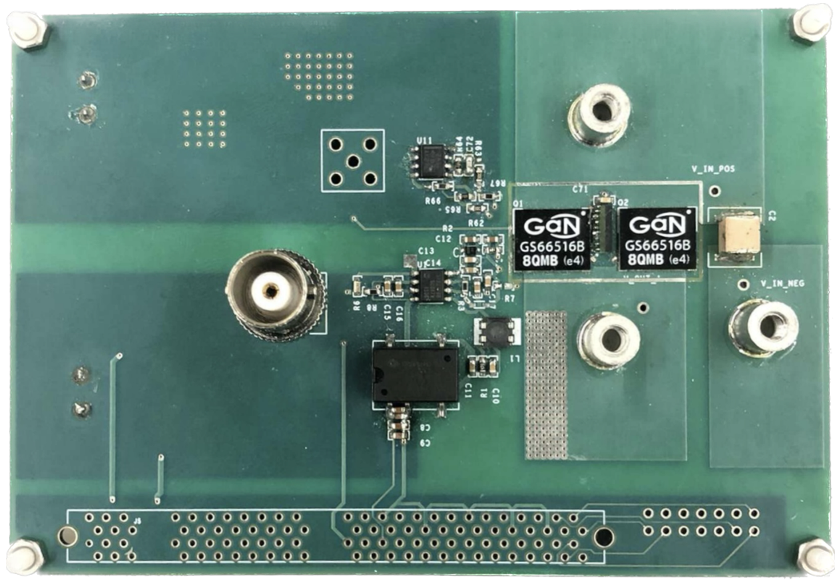

Figure A.1: First protoype of the current mismatch sensor using HMC1051ZL as the detector.

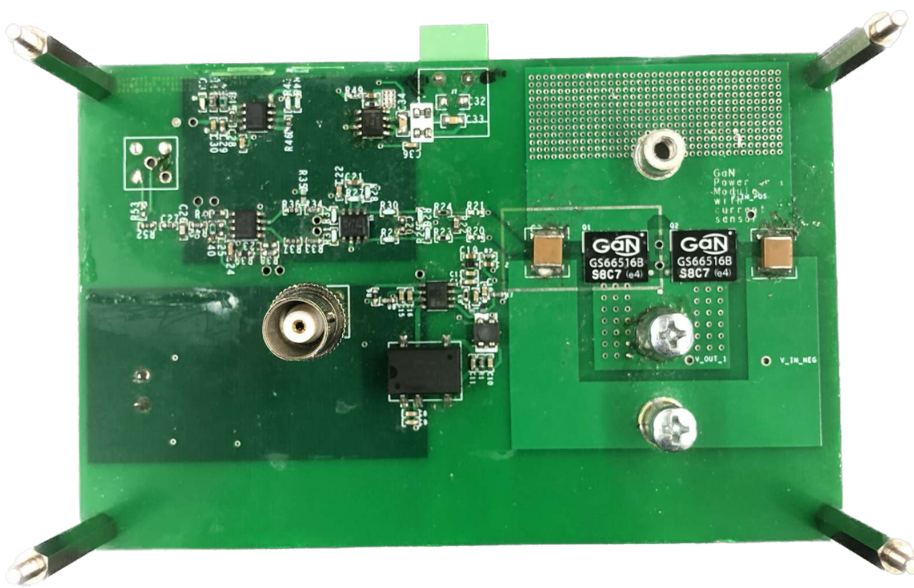

Figure A.2: First protoype of the current mismatch sensor using PCB-embedded spiral Rogowski coil as the detector.

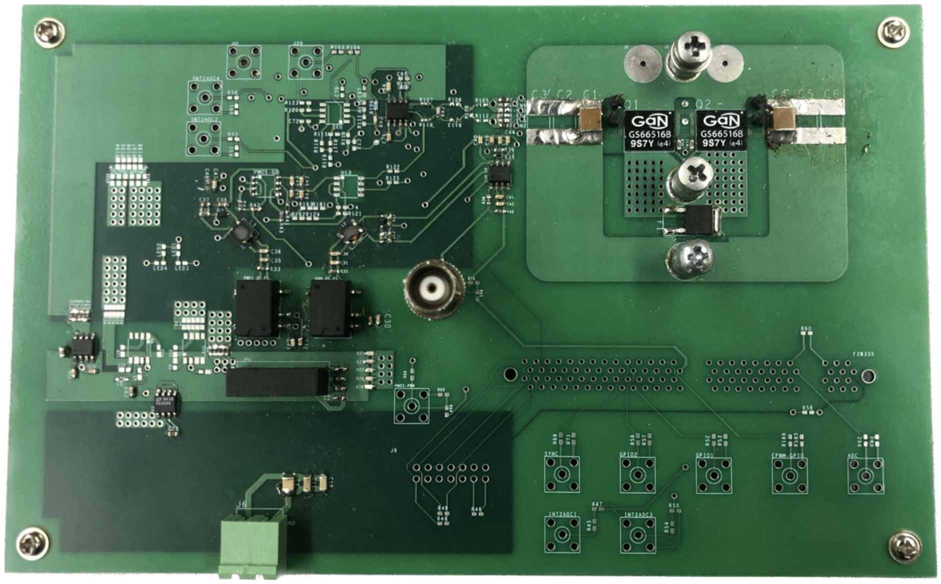

Figure A.3: Second protoype of the current mismatch sensor using PCB-embedded spiral Rogowski coil as the detector.

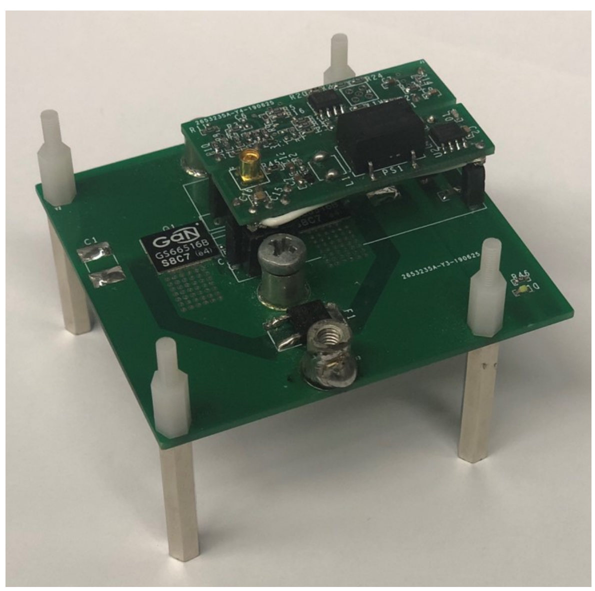

Figure A.4: First protoype of the current mismatch sensor embedded in a stacked module.

Figure A.5: First prototype of the GaN (GS66516B) half-bridge module, including an AMR sensor (HMC1051ZL) as the mismatch detector.

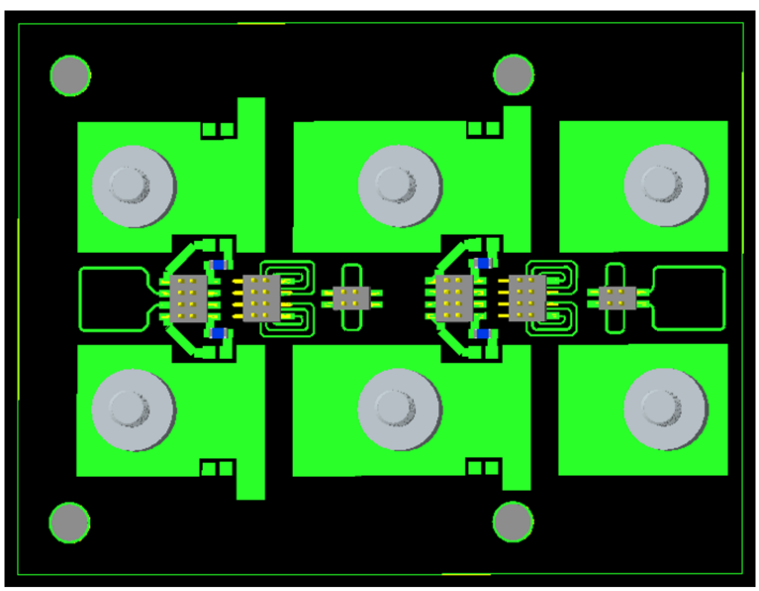

Figure A.6: Layout of a prototyped GaN (GS66516B) half-bridge module, including a Rogowski sensor as the mismatch detector.

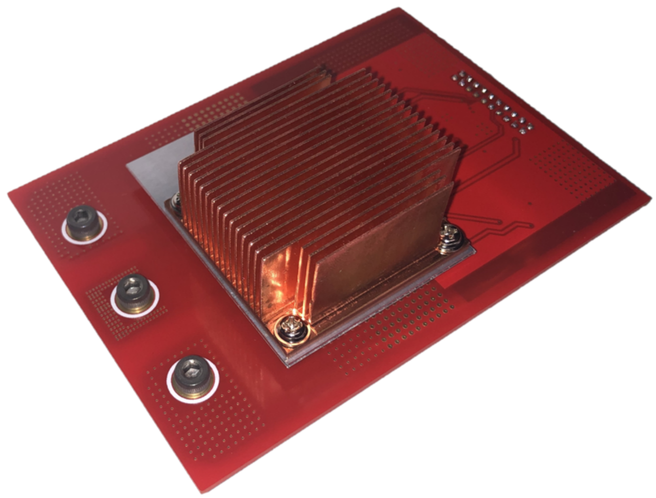

Figure A.7: First prototype assembly of the GaN half-bridge module attached to its gate-driver board (red board).

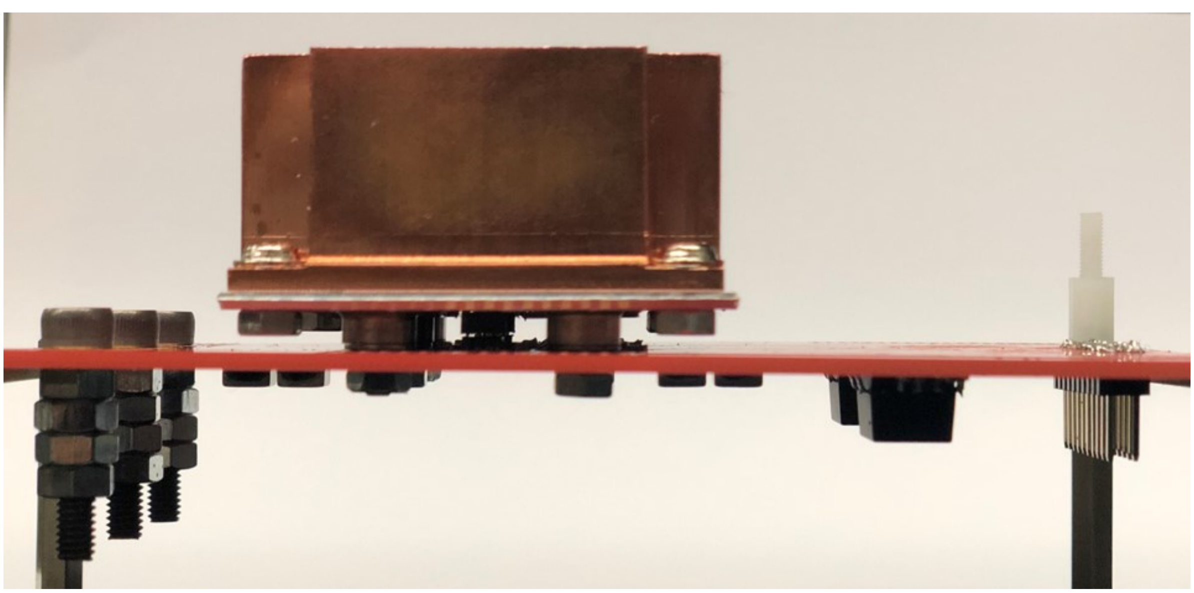

Figure A.8: Side-view of the connections made between the module and gate-driver.

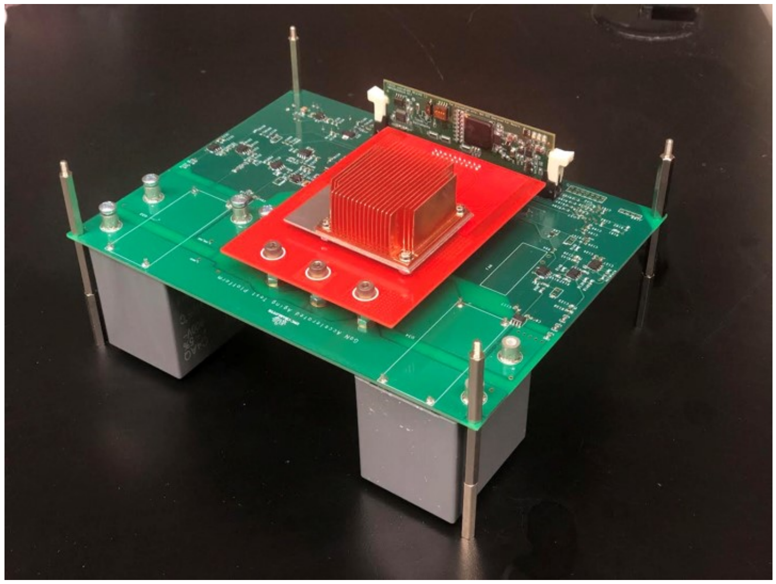

Figure A.9: First complete setup of the half-bridge power module, including gate-driver, as well as the motherboard.

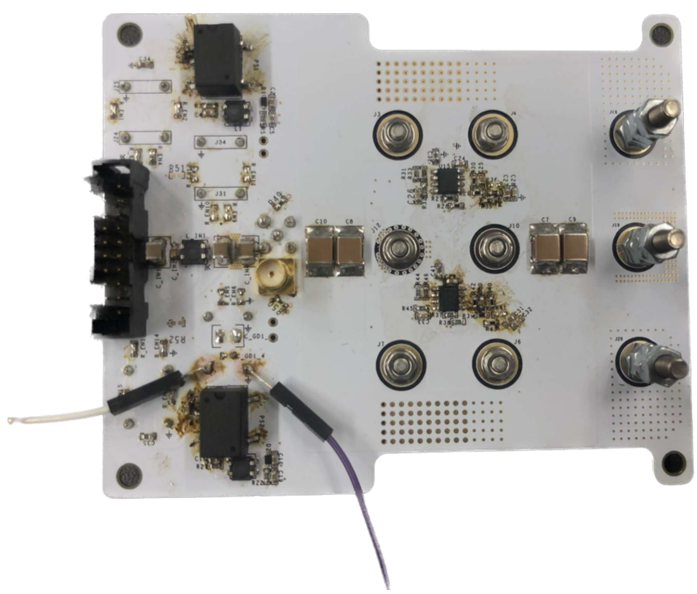

Figure A.10: Second prototype of a gate-driver, including star-ground method.

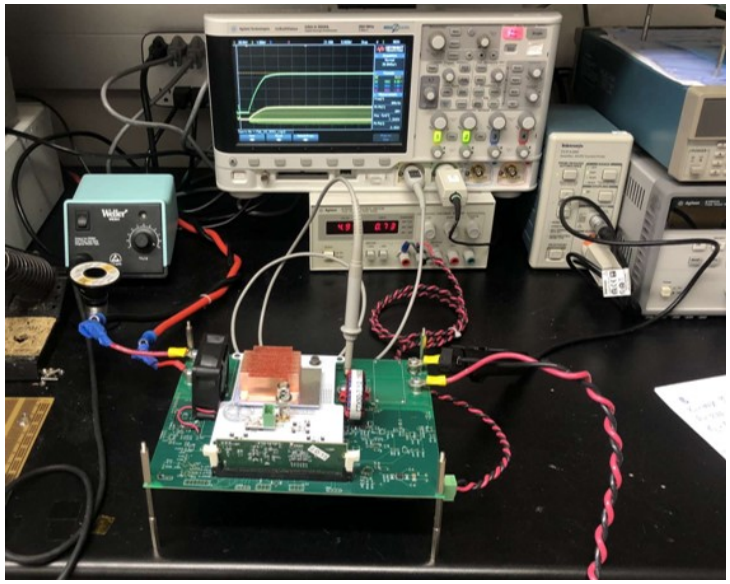

Figure A.11: Boost converter setup experiment, inclduing the latest power module testbed.

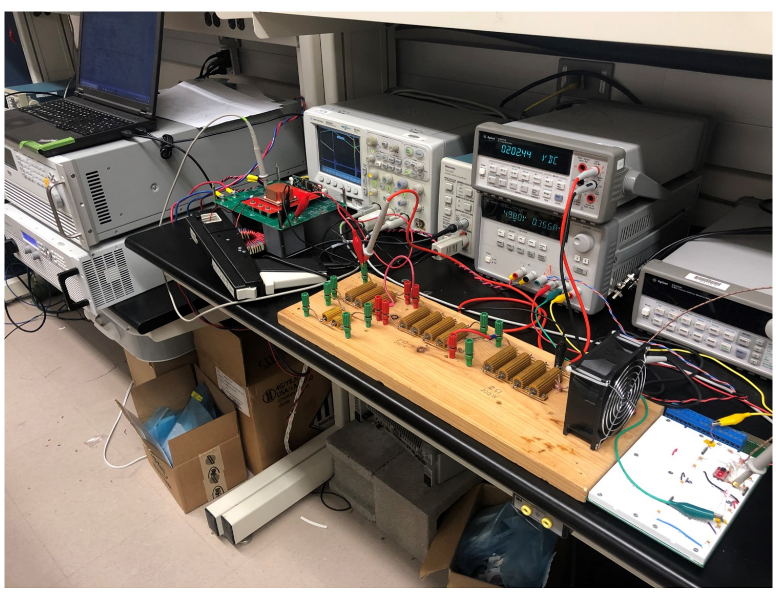

Figure A.12: Second experimental setup for boost converter operation.

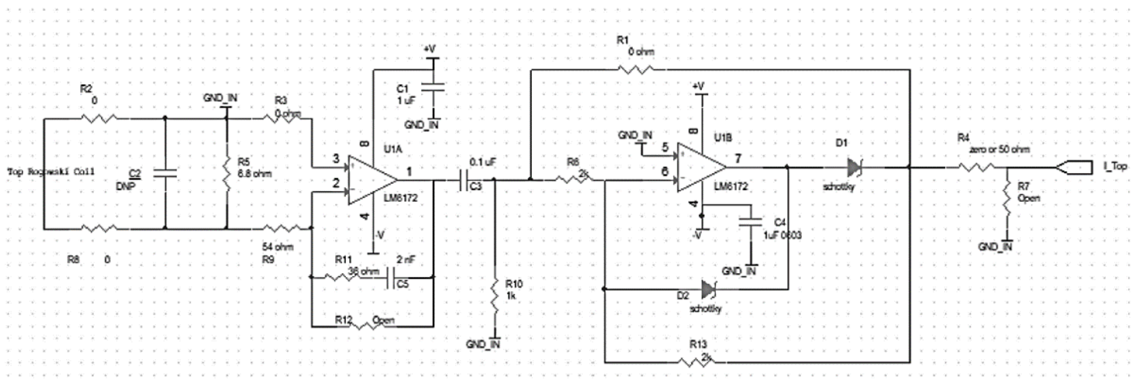

Figure A.13: Schematic of the prototyped uni-directional reset-less Rogowski sensor.

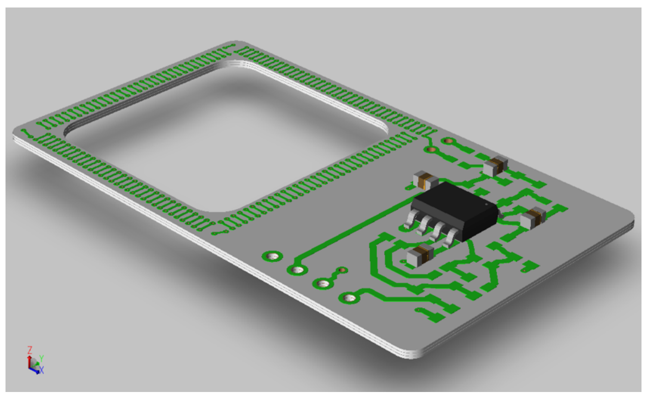

Figure A.14: 3D model of the prototyped PCB-embedded reset-less Rogowski sensor.

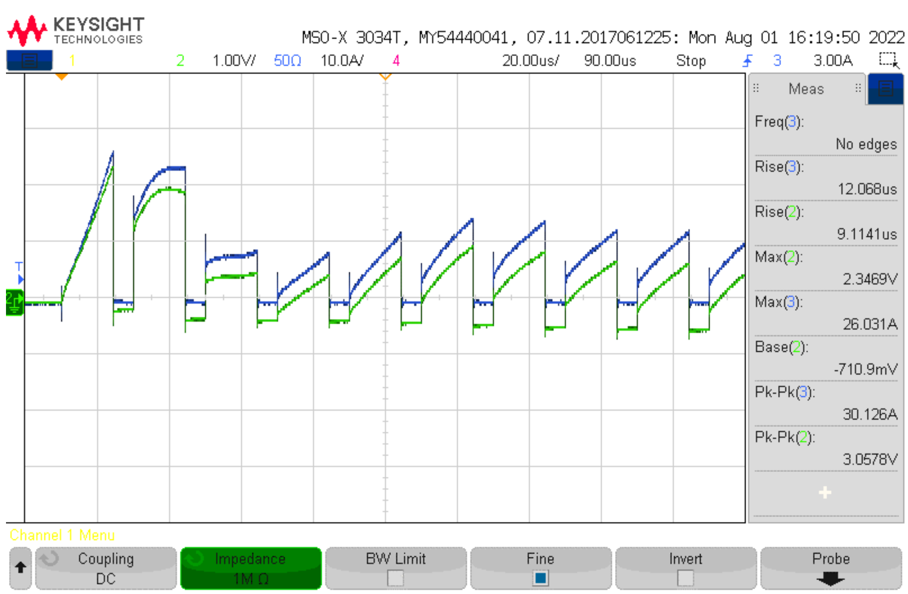

Figure A.15: This figure shows the impact of not having a compensator circuit included with the Rogowski sensor. Blue is the 50 MHz reference current probe. Green is the Rogowski coil sensor output without compensation.

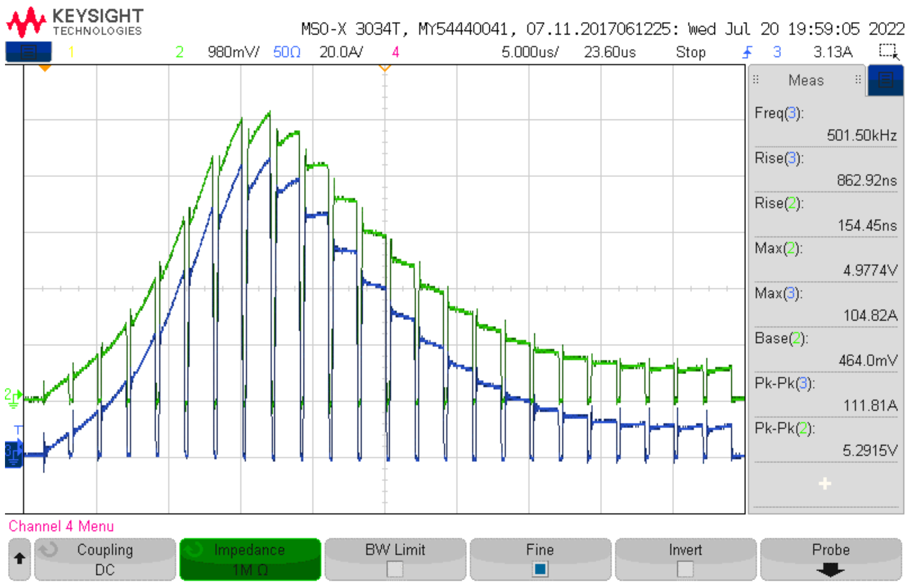

Figure A.16: This figure shows the effectivness of the compensator scheme in correcting the Rogowski coil detector error. The pulse frequency is 500 kHz, while duty cycle is at %90. Blue is the 50 MHz reference current probe. Green is the Rogowski coil sensor output including the proposed compensator circuit.

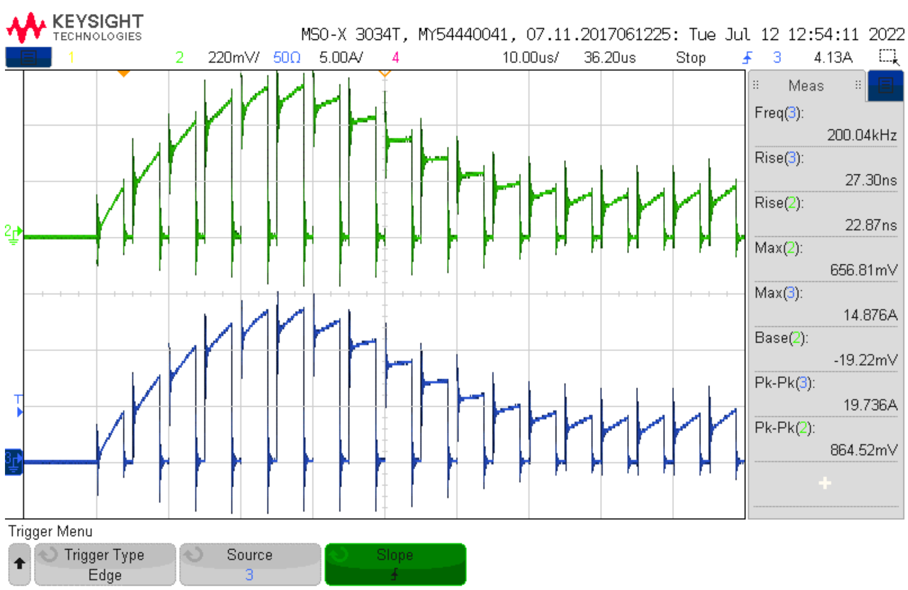

Figure A.17: This figure also demonstrates the compensator scheme performance. The pulse frequency is 200 kHz, while duty cycle is at %90. Blue is the 50 MHz reference current probe. Green is the Rogowski coil sensor output including the proposed compensator circuit.

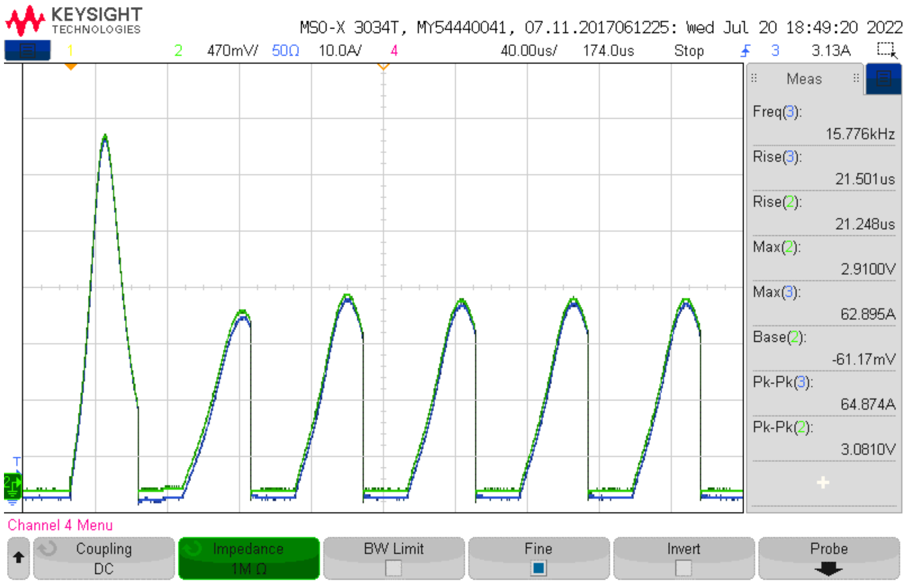

Figure A.18: This figure shows, the sensor is capble of measuring any arbitary unidirectional pulsed signal. Pulse frequency is 15 kHz, while duty cycle is at %60. Green is the Rogowski coil sensor output including the proposed compensator circuit.

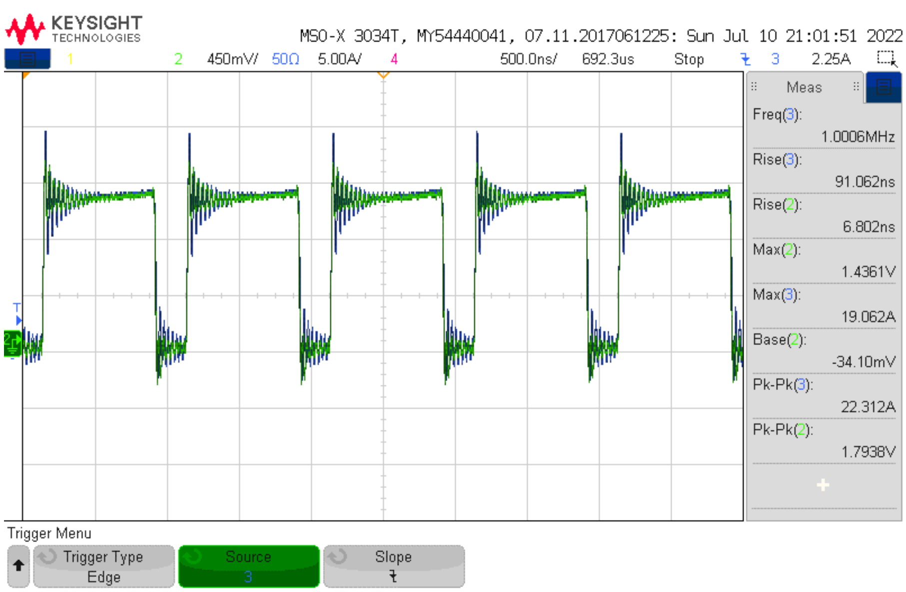

Figure A.19: This figure shows, the sensor is capble of measuring ultra high-frequency signals. Pulse frequency is 1 MHz, while duty cycle is at %85. Green is the Rogowski coil sensor output including the proposed compensator circuit.